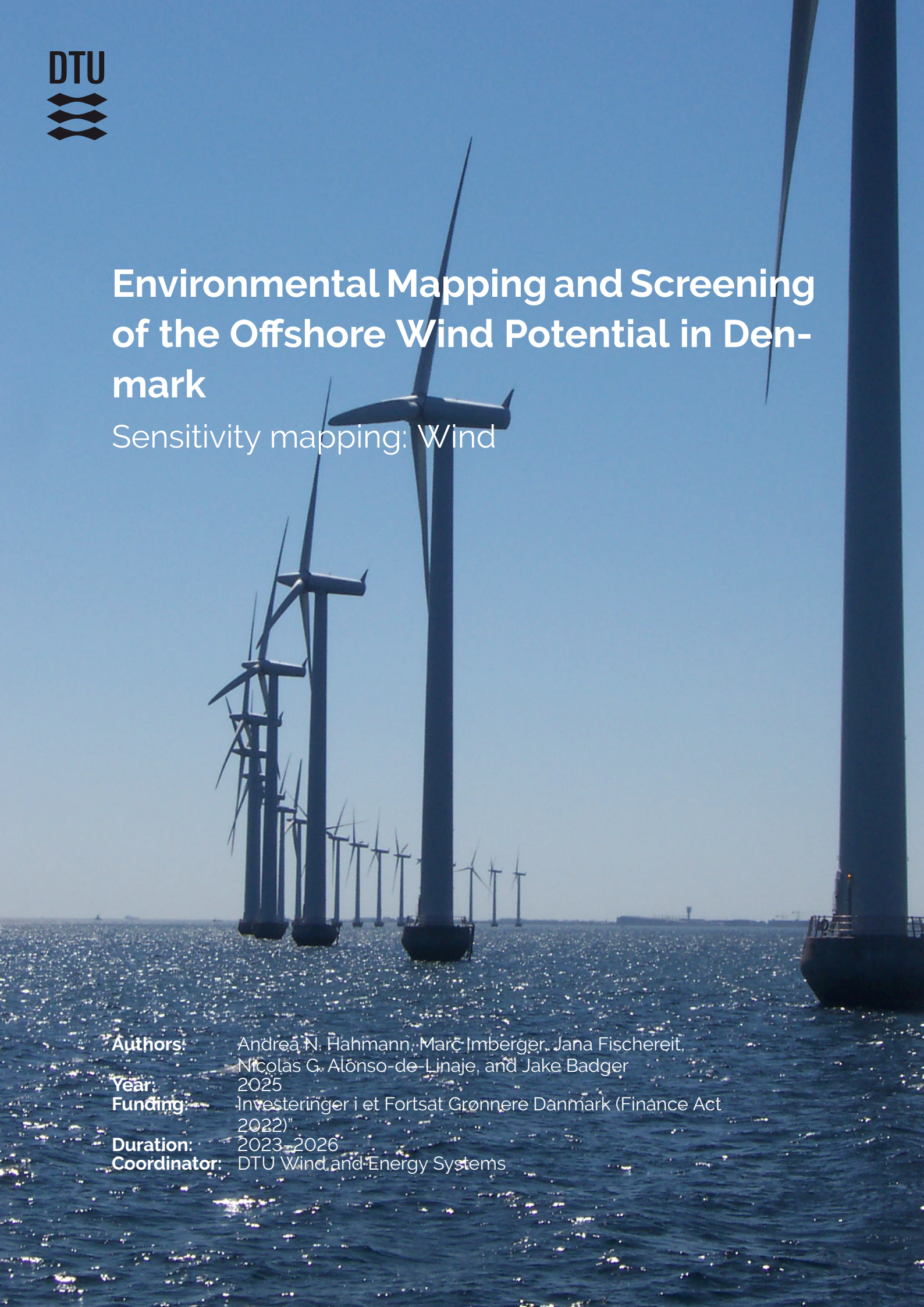

Environmental Mapping and Screening of the Offshore Wind Potential in Denmark

Sensitivity mapping: Wind

Authors: Andrea N. Hahmann, Marc Imberger, Jana Fischereit, Nicolas G. Alonso-de-Linaje, and Jake Badger

Year: 2025
Funding: Investeringer i et Fortsat Grønnere Danmark (Finance Act 2022)"
Duration: 2023–2026
Coordinator: DTU Wind and Energy Systems

Project acronym ENS-DK	**Project Title** Screening af Havvindpotentialet i Danmark	**Project Coordinator** NIRAS
Delopgave #1 Følsom-hedskortlægning	**Deliverable Title** Environmental Mapping and Screening of the Offshore Wind Potential in Denmark	**Version** 4.0
Type Report and Data	**Dissemination Level** Sensitivity mapping: Wind	**Due Date** 01-05-2025
Lead Beneficiary DTU Department of Wind and Energy Systems		**Pages** 44
Lead Author Andrea N. Hahmann (DTU)	**Reviewed by** Jake Badger and Birte Holst Jørgensen	

This report should be cited as:
Andrea N. Hahmann, Marc Imberger, Jana Fischereit, Nicolas G. Alonso-de-Linaje, and Jake Badger (2025), "Environmental Mapping and Screening of the Offshore Wind Potential in Denmark," DTU Public report number DTU E-0255 2025

Disclaimer

Acknowledgements

The authors further acknowledge support from the Danish Energy Agency under the political sub-agreement to the Finance Act 2022 (Investeringer i et fortsat grønnere Danmark).

History of Changes

Date	Version	Author/Reviewer	Comments
17-09-2024	0.1	Andrea N. Hahmann (DTU)	First draft
16-10-2024	0.2	NIRAS and DEA	Review of first version
01-11-2024	1.0	Andrea N. Hahmann (DTU)	Updated text and figures
21-11-2024	1.1	NIRAS and DEA	Second round of comments
20-02-2025	2.0	Andrea N. Hahmann (DTU)	Revised text and data
21-03-2025	2.1	NIRAS and DEA	Third round of comments
13-04-2025	3.0	Andrea N. Hahmann (DTU)	Revised text, added new section
29-04-2025	3.1	Andrea N. Hahmann (DTU)	Revised text
30-04-2025	4.0	Andrea N. Hahmann	Final version

Executive Summary

Operating large offshore wind farms decreases wind speeds in them and their downwind surroundings. This is known as wind farm wake, and it can significantly impact annual energy production, especially in areas with high installed capacity density. To assess this in Danish waters, we use a mesoscale model to capture atmospheric conditions and the effects of wind farms on them, particularly the wind. We simulate the flow to estimate wind resources for the North Sea, South Baltic Sea and the Kattegat using three scenarios: no wind farms, existing farms as of November 2021, and projected deployment in 2030. The 2030 projections were made in the first quarter of 2024. We estimate reductions in wind speed, capacity factors, load hours, and recovery distances for wind speed and changes in other climate conditions.

The main conclusions of this report can be summarised as follows:

- Simulations show that in large wind farms for a 2030 scenario, wind speeds in the southern North Sea may drop by 4 m s^{-1} (corresponding to a reduction in 15 MW capacity factors from 0.6 to 0.2). These reductions are mainly due to the region's high installed capacity density.
- When focusing on the Danish EEZ (Exclusive Economic Zone), existing wind farms and those envisioned for 2030 produce modest reductions in hub-height wind speed and capacity factors compared to other regions in the southern North Sea, owing to strong winds and relatively low installed capacity densities.
- Simulations show that the recovery distances, i.e., the distance required for the wind speed to return to its background value, for offshore large wind farms vary between 20 km to 80 km. This distance depends on the installed capacity density, the size of the wind farm, and the background wind speed. In the Danish EEZ, recovery distances are 20 km to 30 km.
- The modelling results indicate a greater impact on wind speed in large wind farms when using one parameterization rather than the other; however, the recovery distance to the background capacity factor is similar in both simulations.
- The results in this report carry considerable uncertainty, as many aspects of the modelling outcomes remain unvalidated. Comprehensive data needed to validate the simulations is absent, primarily due to the scarcity and availability of extensive observations, and large wind farms similar to those envisioned for the 2030 scenario have yet to be established.
- Simulations show decreases in 2-m temperature (up to 0.2 °C), increases in boundary layer height (up to 120 m), and cloud fractions (up to 7 %). While mean annual changes are not statistically significant at the 95 % level, they may be significant in specific seasons or stability conditions.
- Wind turbines in Denmark would have produced about 20 TW h if driven by the winds simulated by the WRF model and a wind farm parameterization. This aligns reasonably well with the 16 TW h reported by the DEA for 2019–2021, which includes many other losses.

Abbreviations

Acronym	Description
ASL	Above surface level
DEA	Danish Energy Agency
ECMWF	European Centre for Medium Range Weather Forecasting
EEZ	Exclusive Economic Zone
ERA5	ECMWF reanalysis Version 5
EWP	Explicit Wake Parameterization
FITCH	Fitch et al wind farm parameterization
FLH	Full load hours
MYNN	Mellor-Yamada-Nakanishi-Niino boundary layer parameterisation in the WRF model
OSTIA	Operational Sea Surface Temperature and Ice Analysis
TKE	Turbulent kinetic energy
WFP	Wind farm parameterisation
WRF	Weather, Research and Forecasting (model)

Contents

1 Preface

This report contributes to the project "Environmental Mapping and Screening of the Offshore Wind Potential in Denmark" initiated in 2022 by the Danish Energy Agency. The project aims to support the long-term planning of offshore wind farms by providing a comprehensive overview of the combined offshore wind potential in Denmark. It is funded under the Finance Act 2022 through the programme "Investeringer i et fortsat grønnere Danmark" (Investing in the continuing greening of Denmark). The project is carried out by NIRAS, Aarhus University (Department of Ecoscience) and DTU (Department of Wind and Energy Systems).

The overall project consists of four tasks defined by the Danish Energy Agency (https://ens.dk/ansvarsomraader/vindmoeller-paa-hav/planlaegning-af-fremtidens-havvindmoelleparker):

1. Sensitivity mapping of nature, environmental, wind and hydrodynamic conditions.
2. Technical fine-screening and assessment of the overall offshore wind potential based on the sensitivity mapping and relevant technical parameters.
3. Assessment of potential cumulative effects from large-scale offshore wind development in Denmark and neighbouring countries.
4. Assessment of barriers and potentials in relation to coexistence.

This report addresses one component of Task 1: Sensitivity mapping. Specifically, it provides an overview of areas within Danish offshore regions likely to be particularly vulnerable to offshore wind farm development regarding the wake losses of large offshore wind farms based on numerical simulations. Other subjects within Task 1—such as fish, marine mammals, bats, benthic habitats, wind and hydrodynamics, and ecosystem modelling—will be presented in separate reports in late 2024 and early 2025. A synthesis of all topics under Task 1 will be published in 2025.

The overall project has relied predominantly on historical data, with minimal new data collection. As a result, the sensitivity mapping largely depends on the availability and accessibility of pre-existing data across specific subject areas. From the outset, significant effort was made to incorporate all relevant data to address the task requirements comprehensively. Data from the wind and other simulations is used with minimal verification in the modelling tasks, mainly because the required data from specific existing datasets does not exist. Additionally, it is essential to recognise that sensitivity mapping is a dynamic tool that can be updated as new data becomes available.

2 Introduction

Wind energy resources in the North and Baltic Seas surrounding Denmark are vast. Capacity factors for large wind turbines offshore northwest of the Jutland coast are as high as 65 %, one of the most energy-rich regions globally [7]. Denmark has explored this rich resource with five wind farms in the North Sea and eleven wind farms in the Kattegat and Baltic Sea, totalling 2.7 GW of installed capacity in April 2024. In 2023, over half of the Danish electricity generation was produced from wind turbines. Furthermore, onshore wind turbines are one of the cheapest ways to expand power production.

The currently installed wind farms are just a tiny step in decarbonising the Danish energy system, as Denmark has pledged to do by 2050. Because of the abundant wind resources, the country has decided to rapidly expand its offshore wind farms to fulfil its climate change mitigation commitments [12]. However, future wind farms' locations, capacities, and layouts must be strategically planned to maximise energy extraction from the wind. At the same time, the cost and impact on the environment and other economic activities are minimised. Part of the minimisation exercise must include the changes in wind resources caused by the wind farms themselves, as explained in the next section.

2.1 Wind turbine and wind farm wake

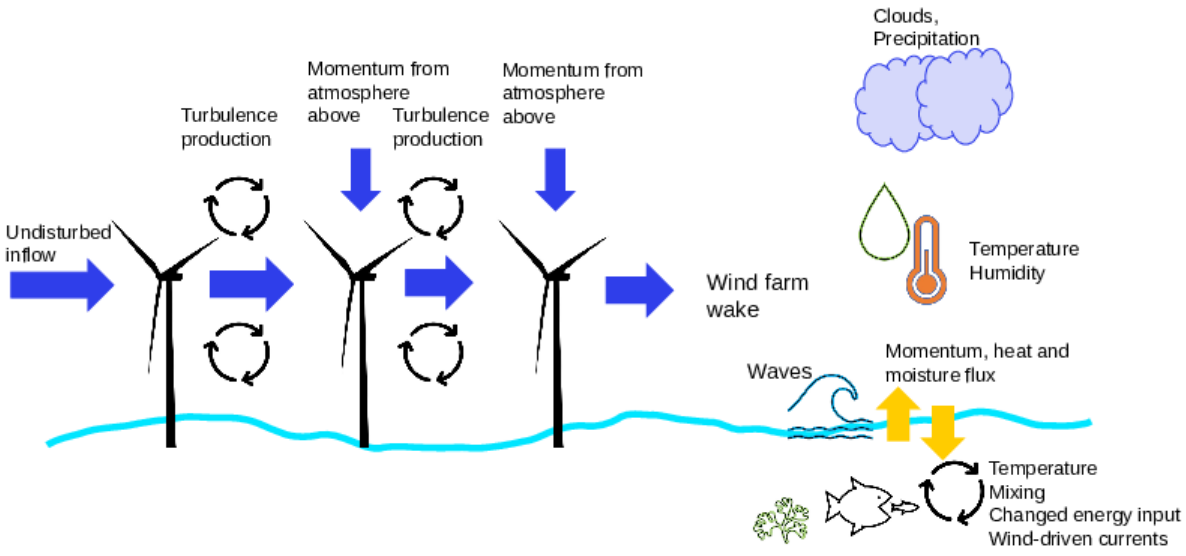

Figure 1: Illustration of the mechanisms at work along a row of wind turbines and the possible environmental effects downstream.

The diagram in Fig. 1 illustrates the simplified mechanisms generating the wind turbine wake. The undisturbed atmospheric flow from the left encounters the first wind turbine, which extracts some kinetic energy from the flow and converts it to electricity, decreasing the wind speed behind it. At the same time, the rotation of the wind turbine blades generates some local turbulence (often called turbulent kinetic energy, or TKE), which diffuses and is transported downstream by the main flow. This mechanism is called the "wind turbine wake". There is a spreading of the wake, which recovers towards free stream conditions when in isolation. However, in wind farms, this modified flow might encounter a second wind turbine, which extracts further energy and generates more turbulence. The enhanced turbulence can mix kinetic energy from above the wind farm and replenish some energy extracted by the first turbine. The mechanism continues downstream, reducing the wind speed and increasing the TKE. More intricate wind turbine layouts complicate the interaction among

the wind turbines. The interaction among the wind turbines depends on whether they align with each other and the dominant wind direction. The layout of modern wind farms is often optimised to minimise energy loss due to the wakes.

In large wind farms, the combined effect of the wind turbines creates a region of reduced wind speed and enhanced turbulence downstream. Physical arguments (i.e., the conservation of mass and momentum) and model simulations have shown that in a massive wind farm, the wind does not stop. Still, some equilibrium is reached between the extraction of energy by the wind farm and the replenishment of energy from above. These mechanisms are often called the "wind farm wake" or the "wind farm wake effect". Wake effects reduce the overall electricity output of a wind farm and potentially any downwind neighbouring wind farms. Wind farms also increase turbulence and the loads on downwind neighbouring wind farms. This could particularly impact areas with a dense concentration of adjoining wind projects. In conclusion, recent observational [32] and modelling studies [34] suggest that when wind energy is used at larger scales, the efficiency of wind turbines is reduced due to wakes, resulting in lower capacity factors and fewer full-load hours [1, 41].

The magnitude of the wind farm wake losses depends mainly on the wind farm's capacity (i.e. the number of wind turbines and their rated power per unit area), the site's wind climatology (frequency distribution of wind conditions), the atmospheric stability, and whether the wind farm is on- or offshore. The more extensive the wind farm and the higher its installed capacity density, the stronger the drop in efficiency and the reduction in wind speed in its wake (e.g. [1, 41]). The stronger the winds, the less the wake effect, especially when winds range well into the rated part of the power curve. The wake effect tends to be more prominent and extensive offshore because the smoother sea surface generates less background turbulence and, thus, creates less mixing of energy from above and less dissipation. Due to the same mechanism, the wake is more pronounced in stable atmospheric conditions (with less turbulence) than in unstable conditions. [1]

When the wind turbines are placed in large wind farms or wind farm clusters (i.e., groups of wind farms), the decrease in wind speed can be significant and extend long distances downstream. Volker et al. (2017) [41] estimated that the wake effect could reduce the annual energy production by as much as 30 % in a large wind farm (i.e., 22 × 22 wind turbines spaced 7 rotor diameters apart) in the North Sea. In a single case study, Ali et al. (2023) [2] reported that wakes from large offshore wind farms could extend 100 km downwind in the southern North Sea.

Wind farms can also affect other atmospheric conditions. Previous studies have shown that the wakes of offshore wind farms might impact surface temperature and other atmospheric properties [21]. Recent studies have also shown the impact of large offshore wind farms on ocean waves [16] and ocean fluxes [35].

Thus, the possible wakes from these large wind farms must be considered when estimating future wind resources. To estimate wind farm wake losses, we use mesoscale models to represent the atmospheric state and its dynamics, and we include the effect of wind farms and wind farm clusters on the atmospheric flow via a simplified model called parameterisation. Because of the nature of the phenomenon, studies in the literature can validate only certain aspects of the wind farm wake with measurements, but not all aspects. Thus, the results presented in this report are "educated estimates" of a possible effect. Also, it is essential to note that the wake losses presented in this report only include those losses from the reduced wind speed in the mesoscale model parameterisations. Other losses, including the wind turbine availability, electrical efficiency, turbine performance, environmental losses, and curtailments, are not included.

[1] Atmospheric stability is a measure of the ability of the air to mix vertically.

3 Mesoscale and wind farm model

The Weather Research and Forecasting (WRF) model [37] is an atmospheric mesoscale model that has become an essential tool for wind resource assessments [30], as reflected in its use for the creation of modern wind atlases [5, 7, 9]. The WRF model can incorporate the effect of wind farms through a wind farm parameterisation (WFP). Several WFPs have been implemented, with the Fitch WFP [17] and the explicit wake parameterisation [EWP, 40] being the two most commonly used [14]. Both WFPs have been extensively discussed in the literature, and research findings are usually framed in comparisons of wind-speed-based wake extension, turbulent kinetic energy (TKE), and power production [2, 4, 20, 34, 36].

3.1 Mesoscale model configuration

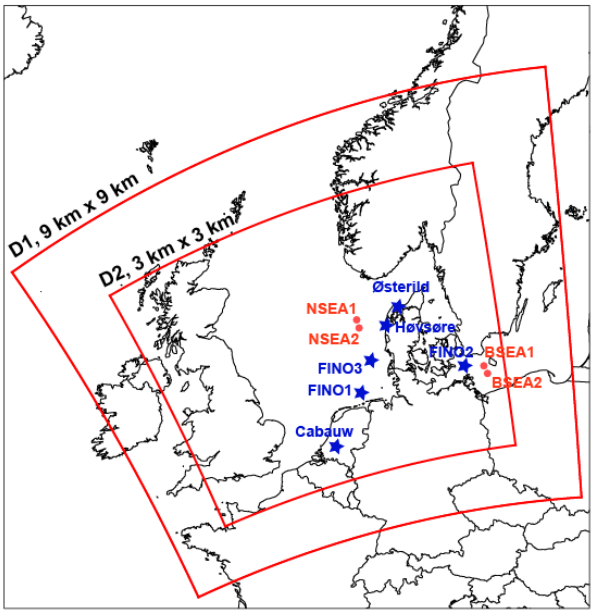

Figure 2: Geographic location of the WRF model domains used in the simulations. The Lidar sites used for validation are shown in red; the mast sites are in blue.

To find the optimal WRF model configuration, we used short-duration simulations of four weeks in January and April 2022, when four floating lidar datasets were available for the North and Baltic Seas. These two periods were chosen based on wind speeds (strong winds in January) and possible low-level jets (April). Note that these periods do not match those of the wind farm simulations. We used a domain centred in the North Sea (Fig. 2) and rotated it to maximise the extent to cover all the Danish waters. The grid spacing of the innermost domain is 3 km by 3 km.

The surface characteristics are critical to the simulation of the wind speed. In particular, the surface roughness length, which determines how "rough" the surface is, is of utmost importance. Thus, we improve the surface characteristics from the default in the WRF model. The land use categories (Fig. 3) are derived from the CORINE dataset, and some land characteristics have been changed from the standard WRF to match the European land cover better. These include the "tidal zone" and "peat bog" (previously named "herbaceous wetland"). The roughness length of forest areas is increased from 0.5 m to 0.9 m. We also aggregate the vegetation properties on each WRF model grid point, thus reducing surface roughness for points close to the coast. The surface roughness of a WRF model grid point is not often 0.9 m because forests do not entirely cover most regions (see Fig. 4).

The particular configuration of the three test simulations is described in Table 1. The general WRF model configuration, including the namelist, is presented in Appendix A. The model evaluation of these three configurations against the lidars and the meteorological tall mast is presented in sec-

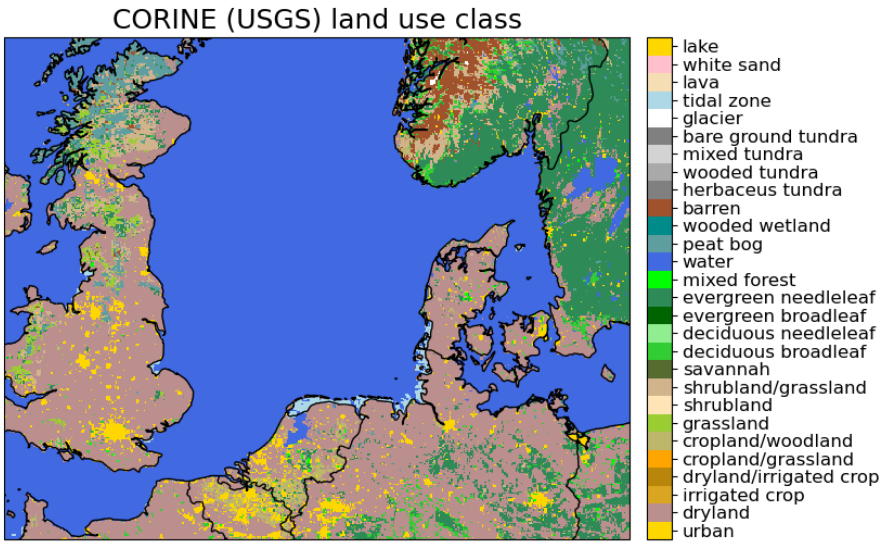

Figure 3: Extent of the inner domain and dominant land use categories used in the WRF model simulations.

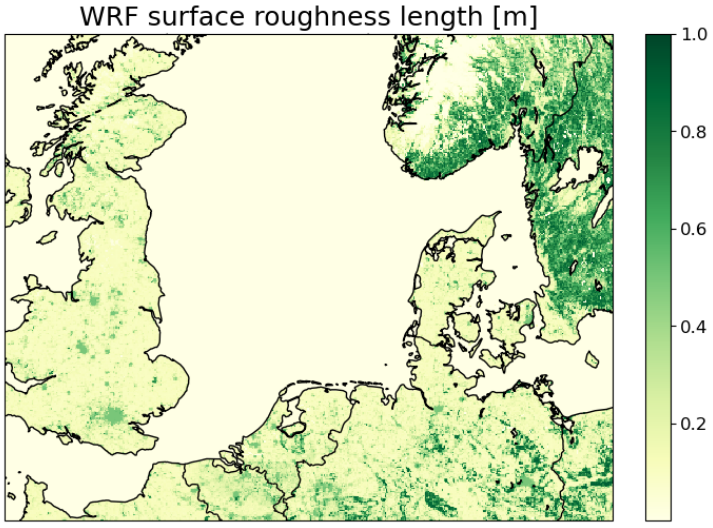

Figure 4: Surface roughness length [m] used in the WRF model simulations.

Table 1: The three experiments used to select the type and number of vertical levels used in WRF model simulations.

Simulation	Model pysics	Parameter setting
SC03-MYNN-MYNN-V01	MYNN PBL, MYNN SL	hybrid sigma-pressure vertical coordinate with 85 levels
SC04-MYNN-MYNN-V02	MYNN PBL, MYNN SL	eta sigma coordinate with 62 levels
SC05-MYNN-MYNN-V03	MYNN PBL, MYNN SL ML=2	hybrid sigma-pressure vertical coordinate with 85 levels

tion 5.1.

The model simulations are run for a single "representative" calendar year. While the chosen calendar year was mainly driven by the availability of measurements in some of the downstream applications, a representative year analysis as described, e.g. [15], has nevertheless been performed to quantify how similar the calendar year is to a "typical year" from a wind energy perspective. "Typical" refers in this context to a year that is representative of the climatological conditions in terms of wind speed (WS), wind direction (WD), and atmospheric stability (STAB) distributions, i.e., the parameters that are relevant for wake effects as described in the introduction. A more detailed description of this process is provided in the Appendix. It was found that 2019 reasonably represents the climatological description of wind direction and our atmospheric stability metric. For wind speeds, it is still adequately representative but shows some over-representation of wind speeds between 5 m s^{-1} to 15 m s^{-1} compared to the climatology. Since this is the range where large wind turbines have the highest thrust to the atmosphere, the wind speed distribution during 2019 leans more towards slightly exaggerating the wake impacts (we would expect to see lower occurrence rates in this wind speed range in the long-term climatology) compared to a "typical" climatological year. However, this overestimation is well within the uncertainty of the simulated wake effects on the flow.

We use data from the European Centre for Medium-Range Weather Forecast ERA5 [26] reanalysis to initialise and provide boundary conditions in the WRF model simulations. The sea surface temperatures and sea ice fractions come from the OSTIA dataset [8, 22] with daily updates as described in the NEWA article [24].

3.2 Wind climate in the model domain

We include the basic wind climatology of the studied area here to facilitate understanding of the interaction between atmospheric flow and wind farms.

Figure 5 shows that in the North Sea, winds mostly come from the southwest to northwest direction, and the dominant wind directions are narrow (from the southwest) in the south but broaden going north. Wind directions are also narrower in winter than they are in summer. When constrained by topographic barriers, i.e., the Dover Strait, the western Baltic Sea, or the Skagerrak) wind roses become more elongated along the direction of the obstacle.

3.3 Wind farm scenarios

The work presented in this report uses the WRF model using the Fitch WFP [17]. To frame these results, we also present the results of an additional wind farm parameterisation developed at DTU, the explicit wake parameterisation [EWP, 40].

The two parameterisations differ in the way they interact with the atmosphere. In the two parameterisations, the WT drag force induced on grid cells across the rotor plane is determined from the WT thrust coefficient and the incident wind speed profile [34]. In the Fitch WFP, a turbine-induced TKE source term is added to the model's TKE equation. The added TKE has been scaled by a factor, namely $C_{\mathrm{TKE}} = 0.25$, as recommended by [3]. In EWP, the added TKE due to the action of the WTs derives solely from the shear-induced in the vertical wind speed profile due to the velocity deficit. Previous studies have found that the spatial extent of wind farm wakes is considerably larger in simulations with the Fitch WFP [20, 34].

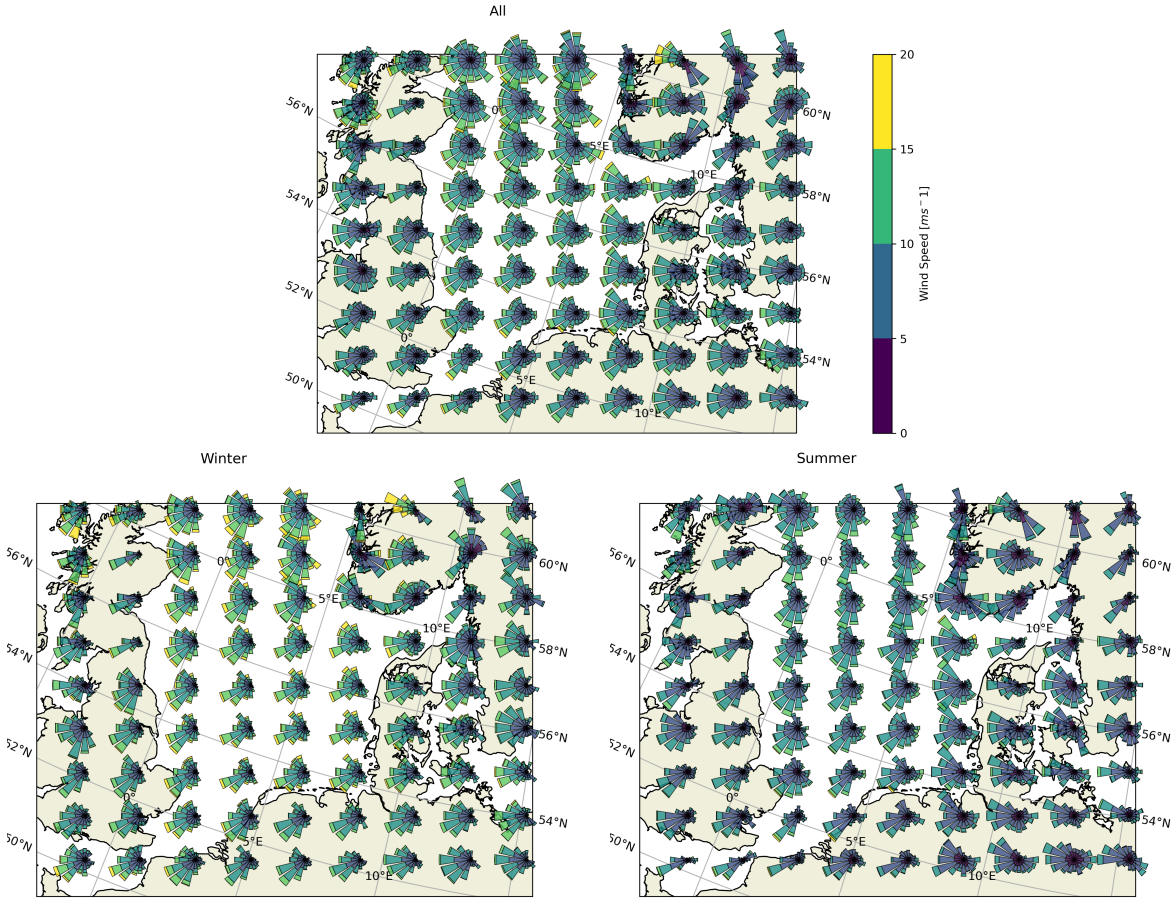

Figure 5: Wind direction distribution as simulated with the WRF model at 150 m above surface level (ASL) for 2019 for the full year (top), winter (lower left), and summer (lower right). The wind direction bins with a bin interval of 5 m s^{-1} are shown by colours on the right; roses are plotted every 35 grid points (~100 km).

Table 2: Scenarios used in the WRF model simulations. The EWP simulations use the EWP wind farm parameterisation to offer a comparison and alternative context in which to view the model results from WFP.

Simulation	Wind farm scenario	Meteorological year
REF_NOFARM	No wind farms	2019
FITCH_CURRENT	Wind farms as of Nov 2021	2019
FITCH_Y2030	Wind farm scenario 2030	2019
EWP_CURRENT	As FITCH_CURRENT, but using EWP	2019
EWP_Y2030	As FITCH_Y2030, but using EWP	2019

We run the WRF model simulations with three wind farm scenarios (Table 2): no wind turbines (REF_NOFARM), wind turbines as of November 2021 (CURRENT), and 2030 scenario (Y2030). The land-based wind turbines do not change from the CURRENT to the Y2030 scenario. Section 4.2 provides more details about the wind turbines. All simulations use identical WRF model configurations. In the wind farm simulations, we introduce the effect of the wind turbines with the distribution of wind turbines as shown in Fig. 6 and Fig. 7. To focus on the Danish waters, Fig. 8 zooms in for improved visibility.

Wind farms on the Danish west coast in the Y2030 scenario vary in installed capacity between 2 MW km^{-2} to 4 MW km^{-2}. The unevenness of the installed capacity in Figure 8 is because the number of wind turbines can vary in each 3 km × 3 km model grid box. This fact should not be relevant to the simulated flow as the model tends to smooth its solution with a few grid points.

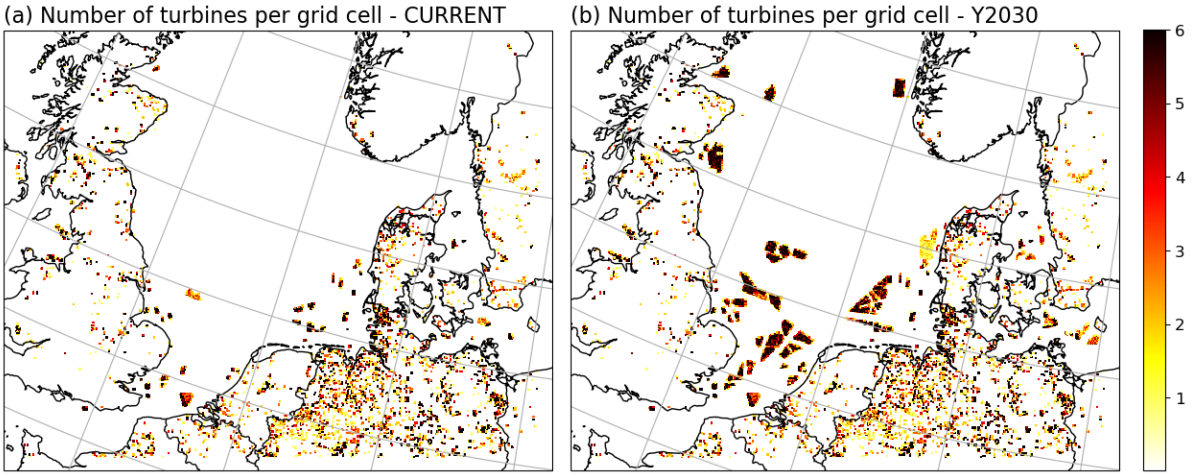

Figure 6: Number of wind turbines per WRF model grid cell in the (a) CURRENT and (b) Y2030 scenarios.

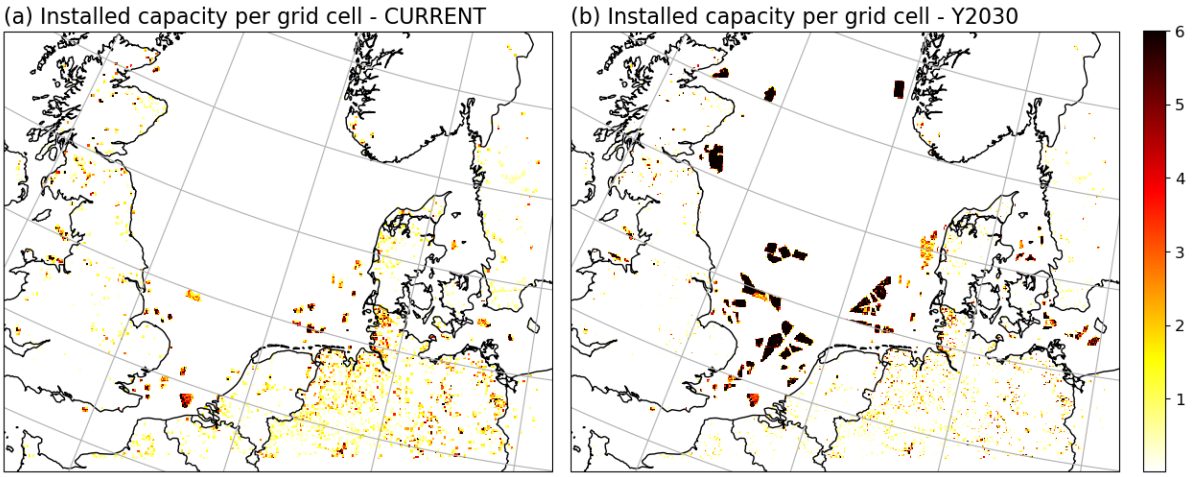

Figure 7: Same as Fig. 6, but for the installed capacity density [MW km^{-2}] in each WRF model grid cell.

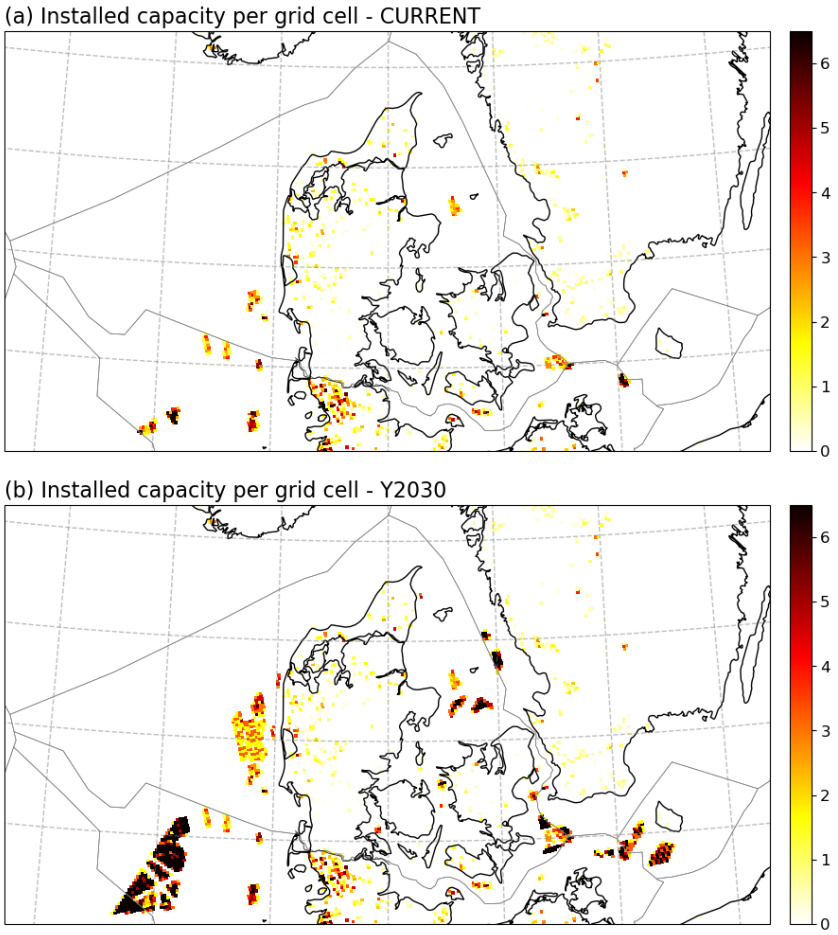

Figure 8: Same as Fig. 7, but zoomed in for the Danish Exclusive Economic Zone and neighbouring waters.

4 Data and methods

4.1 Lidar and tall mast data

Table 3: Measurement instruments, locations, vertical levels, and data availability for 2019 after filtering and resampling for the four Lidar and five mast measurement sites.

Site	Instrument	Latitude	Longitude	Levels	Data avail.
NSEA1	ZephIR ZX300 Lidar	56.6279° N	6.3019° E	30, 40, 60, 90, 100, 120, 150, 180, 200, 240, and 270 m	85 %
NSEA2		56.3444° N	6.4574° E		93 %
BSEA1		54.9944° N	14.3547° E		85 %
BSEA2		54.7170° N	14.5882° E		92 %
Østerild N.	Boom-mounted cup anemometers	57.0870° N	8.8807° E	40, 70, 106, 140, 210, and 244 m	81 %
FINO1		54.015° N	6.588° E	40.3, 50.3, 60.3, 70.3, 80.3, 90.3, 101.2 m	34 %
FINO2		55.007° N	13.154° E	42.4, 52.4, 62.4, 72.4, 82.4, 92.4, 102.5 m	95 %
FINO3		55.195° N	7.158° E	50.55, 70.55, 90.55 m	96 %
Høvsøre		56.441° N	8.151° E	10, 40, 60, 80, 100, 116 m	99 %
Cabauw		51.970° N	4.9262° E	10, 20, 40, 80, 140, 200 m	100 %

We use data from wind lidars and masts in the North and Baltic Seas to validate the control (no wind farm, REF_NOFARM) and current wind farm scenario (CURRENT). We consider measurements from five sites: two offshore floating LiDAR systems (FLSs) in the North Sea (NS1 and NS2), two FLSs in the Baltic Sea (BS1 and BS2), and the Østerild mast in Northern Jutland, summarised in Table 3 and shown in Fig. 2. The data at Østerild has been filtered to remove wind directions affected by the wake of wind turbines at the site from the south direction (133° to 192°). The other masts have been used to evaluate WRF simulations, including farm parameterisations.

4.2 Wind farm data

As part of a project funded by the National Climate Center at the Danish Meteorological Institute (NCKF), a database of wind turbine locations and technical specifications (hub height, rotor diameter, rated power, thrust, and power curves) was created. The database combines information from national datasets [6, 10, 11], a European-wide wind farm database [38], OpenStreetMap [31], and the European Marine Observation and Data Network (EMODnet) [13].

Extensive work was carried out to harmonise and gap-fill the combined dataset, including filling missing data via random-forest-based models and associating wind farm information with individual turbines via a developed wind farm splitting algorithm. However, there are known problems with the data: (1) on land outside SE, DK and DE, we use a combination of windpower.net data (for installed capacities, hub-heights, diameters, etc.) and open street map data (for turbine locations). Windpower.net does report only 3.5 GW for the Netherlands onshore, which is underreported. We have identified a commercial product that could be used to fill in some of the missing data. (2) In the windpower.net database, we will lose additional installed capacity when wind farms are reported inconsistently. In our algorithm, each turbine in OpenStreetMap is mapped to one and only one wind farm in the vicinity. Sometimes, the windpower.net database places several wind farms at identical or very nearby locations without a way of differentiating between them. This problem is worse for some countries than others. Using satellite imagery, a companion project could help improve our

database by directly identifying wind turbine locations, but this does not help with other wind turbine characteristics. It is worth noting that, for Denmark, the quality of the wind turbine data is excellent. Errors in other regions are expected to have minimal effects on the Danish EEZ.

The database contains the location of the wind turbines, the turbine type, hub height, rotor diameter, rated power, cut-in and cut-out wind speed, and turbine power and thrust curve. It also includes the known or reconstructed commissioning and decommissioning dates of the wind farms.

For the Y2030 scenario, DTU received the polygons and installed capacities of the locations of future Danish offshore wind farms from Energistyrelsen. Information for future turbines outside Denmark for the North Sea has been based on information from a preliminary third-party GIS layer (created by the Dutch Rijkswaterstaat (RWS) in October 2023) that Energiestyrelsen shared with DTU and which has been initially developed as part of a cumulative impacts study on the North Sea by Wageningen Marine Research. We have used the provided metadata of the GIS layers on installed capacity and wind farm area information to derive the appropriate number of wind turbines (based on the generic 15MW turbine). At the same time, Energistyrelsen supported mapping wind farms to potential future scenarios (which wind farms should be added to a potential 2030 and 2050 scenario, respectively). It must be noted that the wind farm polygons in the data that was available at the time of creation diverge in some areas from the version that has been published as part of the final version of the study of the cumulative impacts on the North Sea (https://doi.org/10.18174/642357). Potential future offshore wind farms for regions outside Denmark in the Baltic (Sweden and Germany only) have been based on wind farm polygon information from 4Coffshore with input from Energistyrelsen on installed capacities (Sweden) and derived GIS layers of a subset of German wind farms by Energistyrelsen.

With the polygon bounding the area and a target total installed capacity, we fill the polygons with the IEA 15 MW (Fig. 9) using a clustering algorithm to maximise the distance among the wind turbines. The algorithm is based on K-means clustering, where the computed wind farm's total number of wind turbines sets the number of targeted clusters. Finally, the centroid of every cluster gives the wind turbine position when the iteration process converges. Small wind turbines whose rotor diameter (rotor diameter < 54 m) and hub height (hub height - half rotor diameter is less than 18 m) cannot be adequately represented by the vertical structure of the WRF model grid have been removed.

Table 4 summarises the resulting installed capacity by country in the WRF model simulations. The most significant increase is by Great Britain, more than 10-fold, from 10.2 GW to 109.5 GW. Denmark's installed capacity increases more than 7-fold, from 2.3 GW to 17.0 GW. Due to the abovementioned problems, installed capacity in some countries could be underrepresented. The current offshore capacity in Great Britain, for example, is underrepresented (other sources report ~26 GW in 2021 for all regions (with some not covered in our simulations), while the 2030 target appears to be overestimated. The offshore wind farms off the coast of Scotland are extensive and of very high installed capacity density (~12 MW km^{-2}). If approved, the Berwick Bank Wind Farm project alone will provide 4.1 GW of installed capacity.

Table 4: Installed capacity (in GW) per country in the CURRENT (November 2021) and 2030 in the WRF model domain. CURRENT is the current (November 2021) scenario, and Y2030 is the 2030 offshore wind farm scenario.

Country	Onshore CURRENT (2021) and 2030 [GW]	Offshore CURRENT (2021) [GW]	Offshore Y2030 [GW]
DK	2.5	2.3	17.0
SE	2.1	0.1	2.4
DE	31.9	7.3	29.4
GB	7.9	10.2	109.5
NL	2.4	2.6	38.1
NO	1.2	–	10.0
PL	0.4	–	–
BE	1.1	1.9	1.9
FR	0.9	–	–
Total	50.4	24.4	218.0

4.3 Capacity factor

The capacity factor (CF) is the ratio of the electrical energy produced by a wind turbine for the period considered to the electrical energy that could have been produced at continuous full-power operation during the same period. For the North Sea, capacity factors vary between 0.45 in the south and 0.7 in the Skagerrak for a modern offshore wind turbine (e.g., 15 MW).

In this study, we use the IEA 15 MW reference turbine (Fig. 9, [19]) as a reference for capacity factor calculations and as the turbine used in the future wind farms offshore in the 2030 scenario. This turbine has a proposed hub height of 150 m and a rotor diameter of 242 m, spanning heights from 29 m to 271 m, nearly matching the FLSs scan levels (30 m to 270 m). The turbine has a cut-in and cut-out wind speed of 3 m s^{-1} and 25 m s^{-1}, while rated power is reached at 10.59 m s^{-1}. We compute the CF using the simulated wind speed at 150 m.

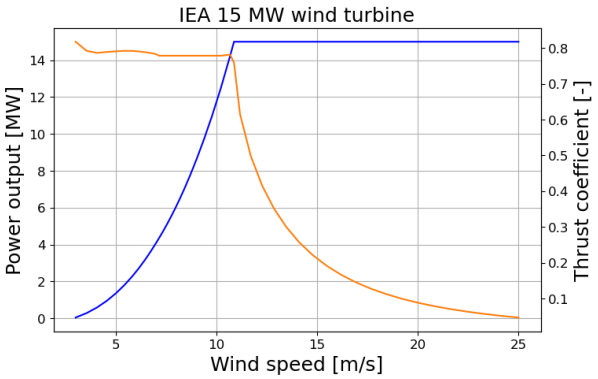

Figure 9: Power and thrust curve of the IEA 15 MW reference wind turbine.

5 Model evaluation

5.1 Evaluation of the control simulations

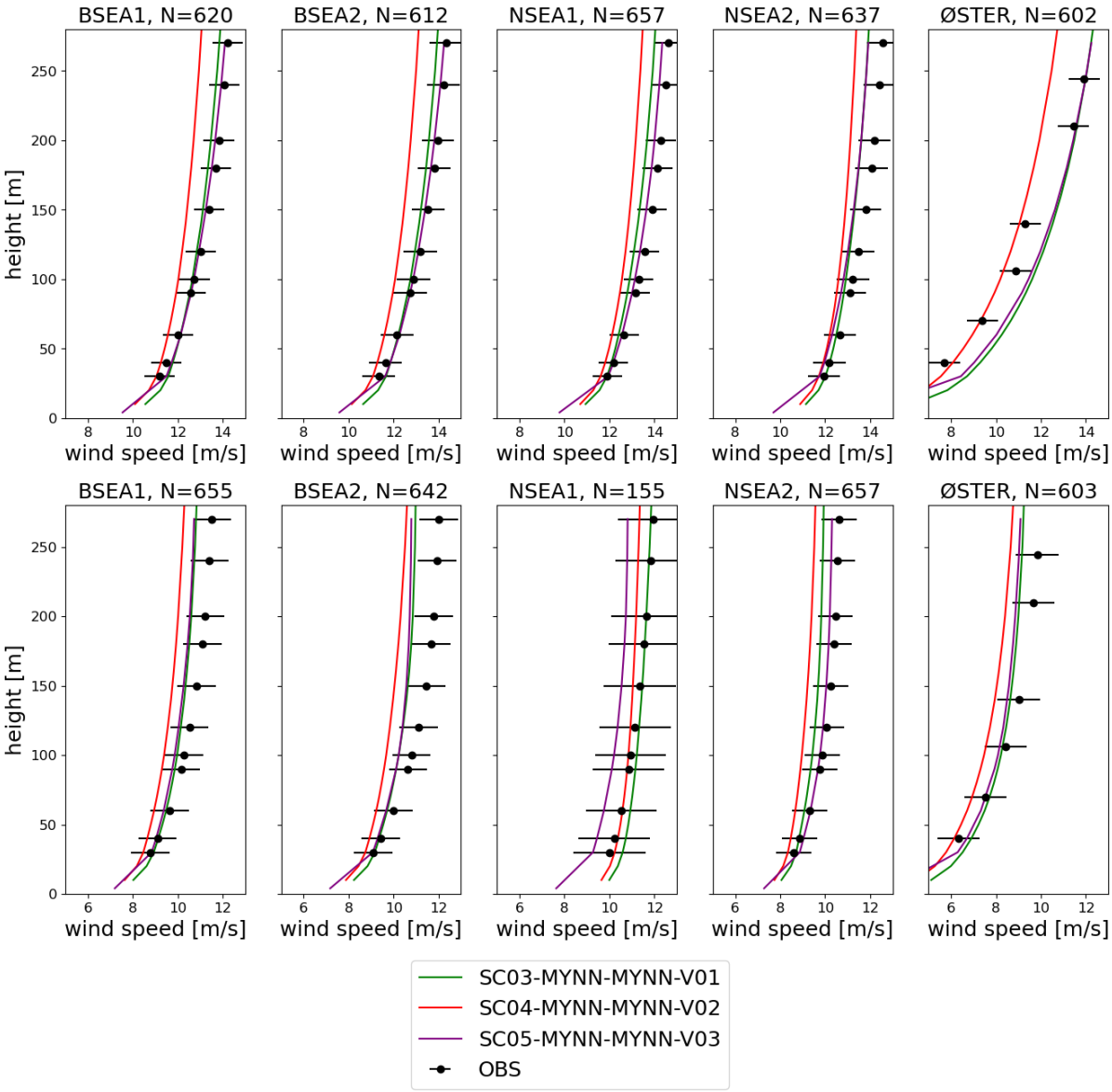

Figure 10: Evaluation of the wind profile of model-simulated mean wind speed against measurements at the five observational sites in Fig. 2 for two time periods: 2022-01-01 to 2022-01-28 (top row) and 2022-04-01 to 2022-04-28 (bottom row). The number of samples used for each profile is written at the top of each plot. The error bars in the estimated mean of the observed wind speeds are determined through circular block bootstraping[28]

In the simulations using the wind farm parameterisation, the WRF model configuration limits us to one planetary boundary layer (PBL) scheme. However, we can choose other parameters to improve performance. To decide on an optimal configuration for the simulations, we tested three setups for two 28-day periods during 2022, all without wind turbines, in the experiments described in Table 1. The results for the five sites in Fig. 2 and Table 3 are shown in Fig. 10. For January, there is good agreement between models and observations in all sites, favouring the SC05-MYNN-MYNN-V03 experiment at most sites, except for Østerild where the wind measurements are influenced by the land characteristics below 150 m. The conclusions are unclear in April, with not-so-good agreement

above ~120 m in all experiments and nearly identical profiles between SC03-MYNN-MYNN-V01 and SC05-MYNN-MYNN-V03 at BSEA1, BSEA2 and ØSTER. SC03-MYNN-MYNN-V01 is best at NSEA1, but the data availability is low ($N = 155$). The lack of performance for the sites in April, especially in the Baltic Sea, is probably related to the misrepresentation of low-level jets (a fast-moving ribbon of air in the low levels of the atmosphere), as shown in Olsen et al. (2024)[29].

In conclusion, the WRF model configuration SC05-MYNN-MYNN-V03 was chosen for all year-long simulations. Other WRF model configurations perform better at these sites [29]. However, we are confined to the MYNN planetary boundary layer scheme [27] because it is the only one that can be used with the two wind farm parameterisations needed in this study. The under-prediction of the wind speeds at the height of the wind turbine rotor implies that the relative wake losses are over-predicted.

In the data delivered to the project, we used the Fitch parameterisation because it is the most widely used and tested. In addition, studies have shown that the parameterisation shows more consistent results with measurements very close to the surface [25]. It is essential to accurately predict the surface winds for further downstream applications by Aarhus University for hydrodynamic modelling and NIRAS as input to the wave model, which uses the simulated surface wind speeds. However, using the Fitch WFP significantly impacts the atmospheric flow (i.e., deeper wakes). The underprediction of the wind speeds and choice of wind farm parameterisation imply that the wake losses are likely overpredicted. Consequently, the results regarding the wind speed deficits and horizontal extension of the simulated wakes should be considered cautiously.

5.2 Evaluation of the WRF model when using a wind farm parameterisation

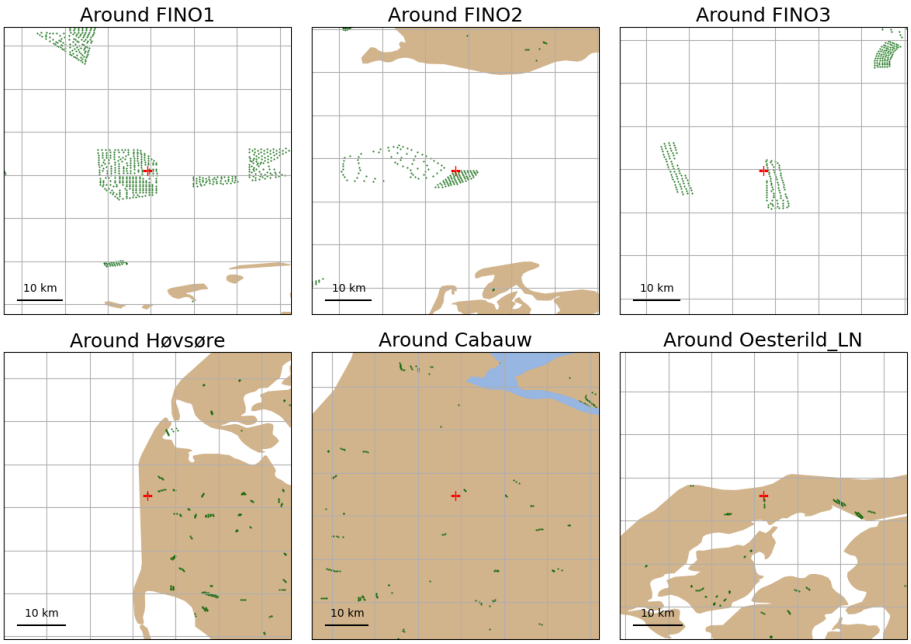

Figure 11: Land and offshore wind turbines in the WRF model simulations around each mast location (red cross) used for model validation. The green dots indicate turbine locations.

Verifying wind farm parameterisations is challenging because there are very few observations offshore, and it is often not possible to simultaneously evaluate the changes in wind speed due to wind turbines and the power produced by these turbines. We take a simple approach here and consider only the effect on the wind speed. In total, data from six tall masts are used for validation. The mast sites FINO1, FINO2 and FINO3 had operating wind farms in their vicinity during 2019 (Fig. 11). Thus, Fig. 12 shows the simulated wind speed at these three sites when wind turbines are included (CURR EWP, CURR FITCH) or not (NoWF) in the simulations. To compare and evaluate the modelling simulations when turbines are absent, at Høvsøre and Cabauw, no wind turbines exist in the WRF model

simulations near the masts.

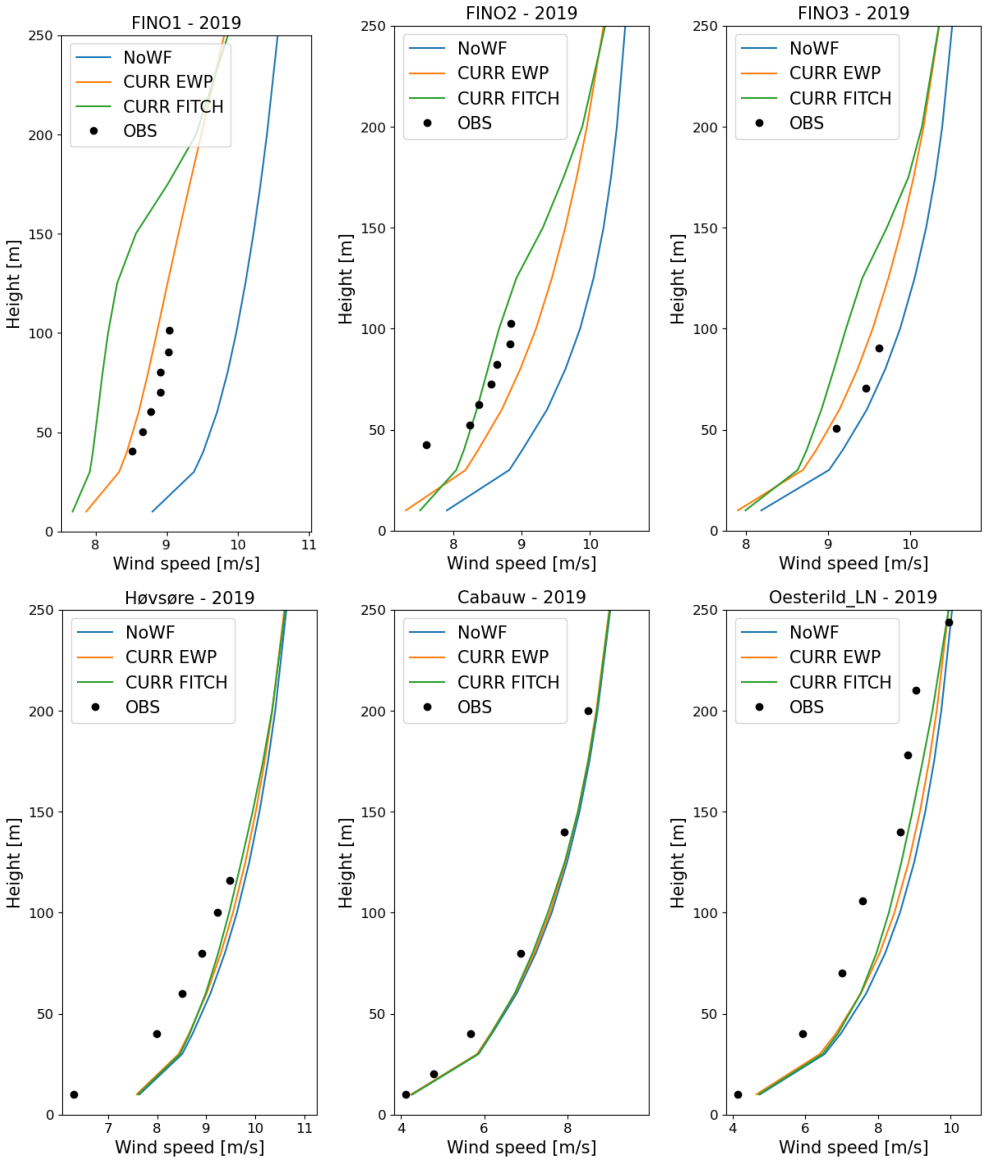

Figure 12: Mean wind speed as a function of height observed and simulated during 2019 for the six mast sites in the North and Baltic Seas in Table 3. The simulations are for two WFPs (Fitch and EWP) with the CURRENT wind farm scenario (Table 2). The observations and model simulations are always colocated in time.

The six sites chosen have different characteristics. The three offshore sites are near large wind farms, particularly FINO1, where most wind farms are upstream of the most frequent wind direction. FINO1 is in the near wake region for winds from the west. At FINO2, the meteorological mast is near a wind farm, which is not situated along the dominant wind direction. Similarly, FINO3 is close to a wind farm but not in the main wind direction. The closest wind farm along the main wind direction is around 15 km upstream. Wind turbines at Høvsøre are north of the mast location, but this wind direction is uncommon. At Østerild, a row of wind turbines exists south of the mast. No wind directions have been excluded from the model assessment. No significant wind turbines surround the Cabauw location.

Figure 12 shows the effect of the WFP on the flow for these three sites. At FINO1, the WFP reduces the mean wind speed by about 1.2 m s^{-1} to 2.0 m s^{-1} at the heights where the wind turbine's blades intersect the flow. Here, the EWP scheme better matches the simulation to the observations identified in previous studies [20]. At FINO2, only EnBW Baltic 2 (east of the mast) was operational in 2019 (Kriegers Flak to the west was commissioned in 2021 but was still included in the simulations).

At this location, the WFPs overestimate the wind speed deficit of the wind farm, but the shape of the wind profile is well simulated by the model using the EWP scheme. At FINO3, the wind farms Sandbank (~15 km west, 288 MW) should contribute most to the wake effect, while DanTysk (east, 288 MW) is often downstream from the meteorological mast. The wind speed reduction due to the wind farm at FINO3 is in the order of 0.5 m s^{-1}.

At the three land meteorological masts, Høvsøre, Cabauw and Østerild, the effect of the wind farms should be small and only felt in unusual wind directions: from the North and NE in Høvsøre and the south in Østerild. At Østerild, the effect of the very tall wind turbines is apparent in both simulations with WFP. The mean wind speed profile is reasonably well simulated at turbine-operating heights. However, for these land sites, the previously identified biases (section 5.1) are now in the opposite direction; the WRF simulations overestimate the mean wind speed at the three sites, especially at heights close to the surface.

In conclusion, the WFPs reasonably reduce the wind speed felt at the three offshore mast sites. However, the number of validation sites and the conditions are too uncertain to conclude which WFPs, Fitch, or EWP are most accurate. For this report, it seems reasonable to assume that the most accurate answer regarding wind speed prediction lies between the WRF model simulations using the two wind farm parameterisations.

6 Results

6.1 Difference maps

Here, we present the difference maps for various quantities as annual means (all months in 2019) or seasonal means: winter (average of January, February, and December) and summer (average of June, July, and August). In all the plots, the first column is for the Fitch WFP; the second is for the EWP WFP. The differences are always for the simulations using the Y2030 scenario minus the CURRENT scenario. The averages are of all time periods in a year. The plots zoom in on the Danish Exclusive Economic Zone (EEZ); figures for the entire domain are shown later in Section 6.1.3.

For the figures focusing on the Danish EEZ, we analyse relevant wind energy quantities, such as wind speed and capacity factors. Other climate-relevant quantities, such as temperature, boundary layer height and cloud fractions, are analysed only for the whole domain. The changes in these quantities are small within the Danish EEZ but could be relevant to other modelling activities in the project.

Wind speed

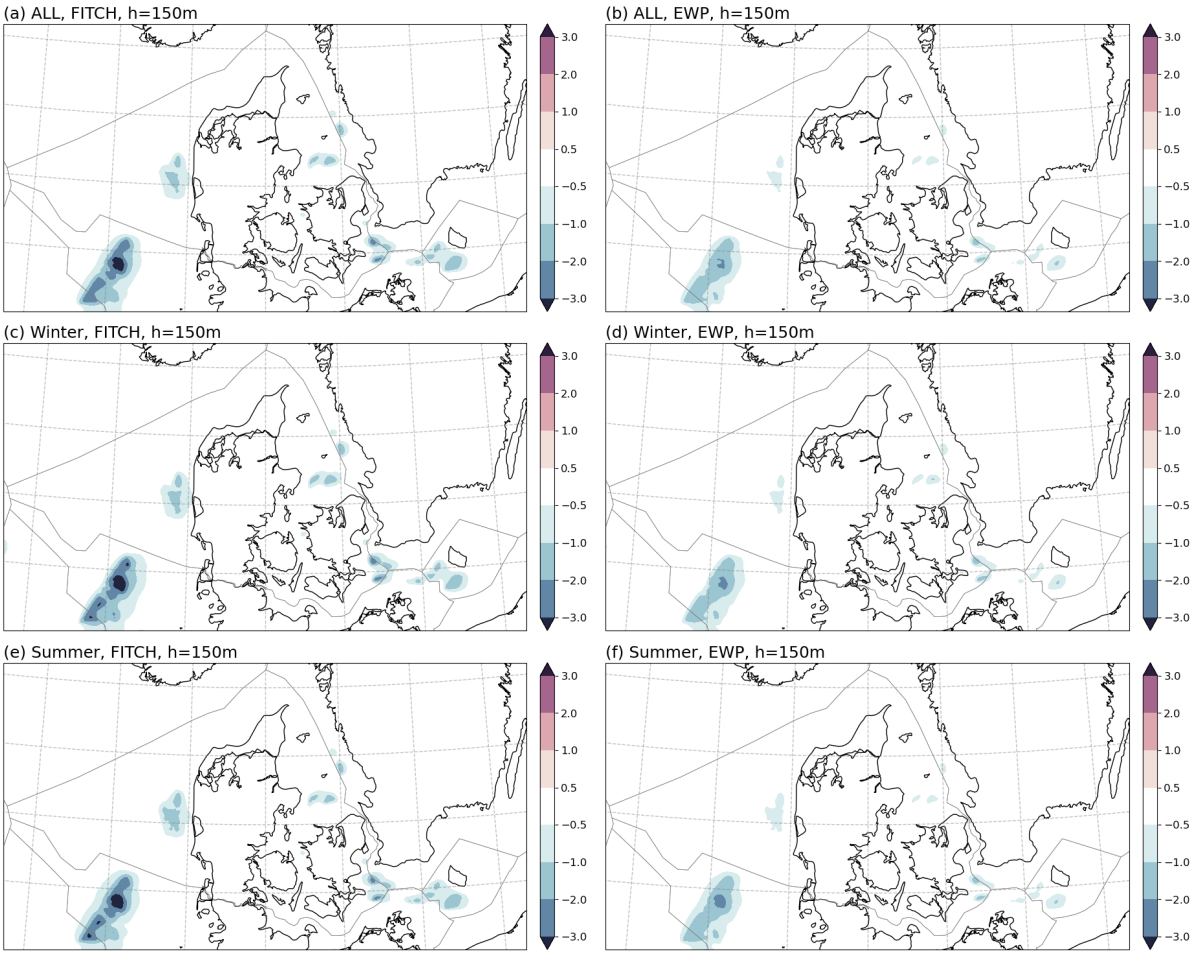

Figure 13: Wind speed difference [m s^{-1}] at 150 m ASL between the Y2030 and CURRENT wind farm scenario for 2019 for the Fitch (a, c, and e) and EWP (b, d, and f) WFPs for the full year (a and b), winter (c and d) and summer (e and f).

The differences in mean wind speed at 150 m ASL and 10 m ASL are presented in Fig. 13 and 14, respectively. For this region at 150 m, differences are largest for the simulation using the Fitch WFP in winter with maximum values of −3.9 m s^{-1} at the proposed cluster of wind farms in the German waters. In the Danish waters, differences in wind speed are at most −1.2 m s^{-1} in the North Sea and −1.5 m s^{-1} in the Baltic Sea in the simulations using the Fitch WFP. The area affected by wind speed

changes beyond −0.5 m s^{-1} in both parameterisations is similar. This effect will be easier to see in the transects presented in Section 6.2.

At 10 m, the wind speed deficits mirror those at 150 m, but with lesser magnitude. Here, the most significant changes are −1.0 m s^{-1} in the FITCH simulations during winter (Fig. 14c). In the Danish waters, the most significant differences are found in the Baltic Sea in the Kriegers Flak region, where changes in 10-m wind speed can be as large as −1.0 m s^{-1} during the summer in the simulation using the EWP scheme (Fig. 14f).

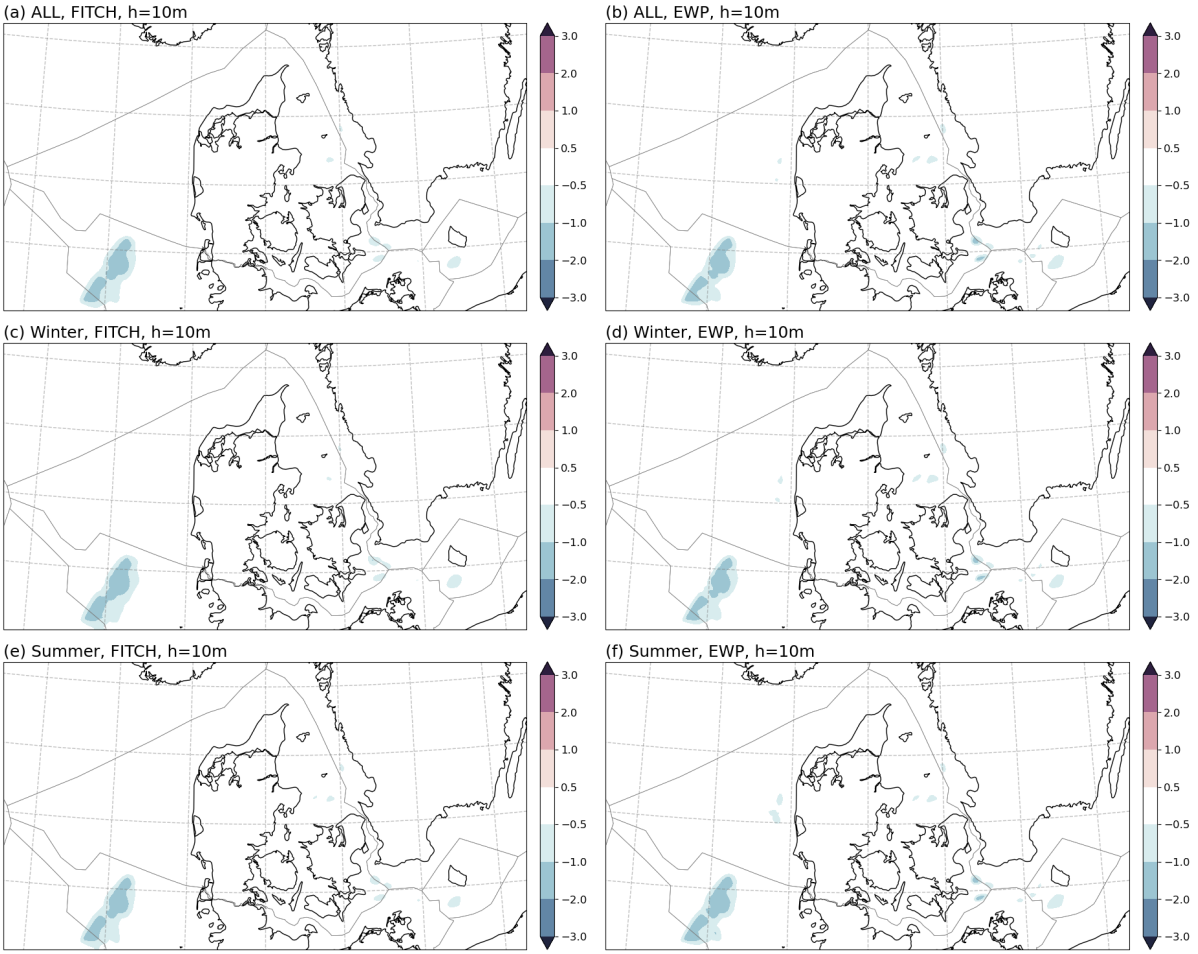

Figure 14: Wind speed difference [m s^{-1}] at 10 m ASL between the Y2030 and CURRENT wind farm scenario for 2019 for the Fitch (a, c, and e) and EWP (b, d, and f) WFPs for the full year (a and b), winter (c and d) and summer (e and f).

15 MW Capacity factor

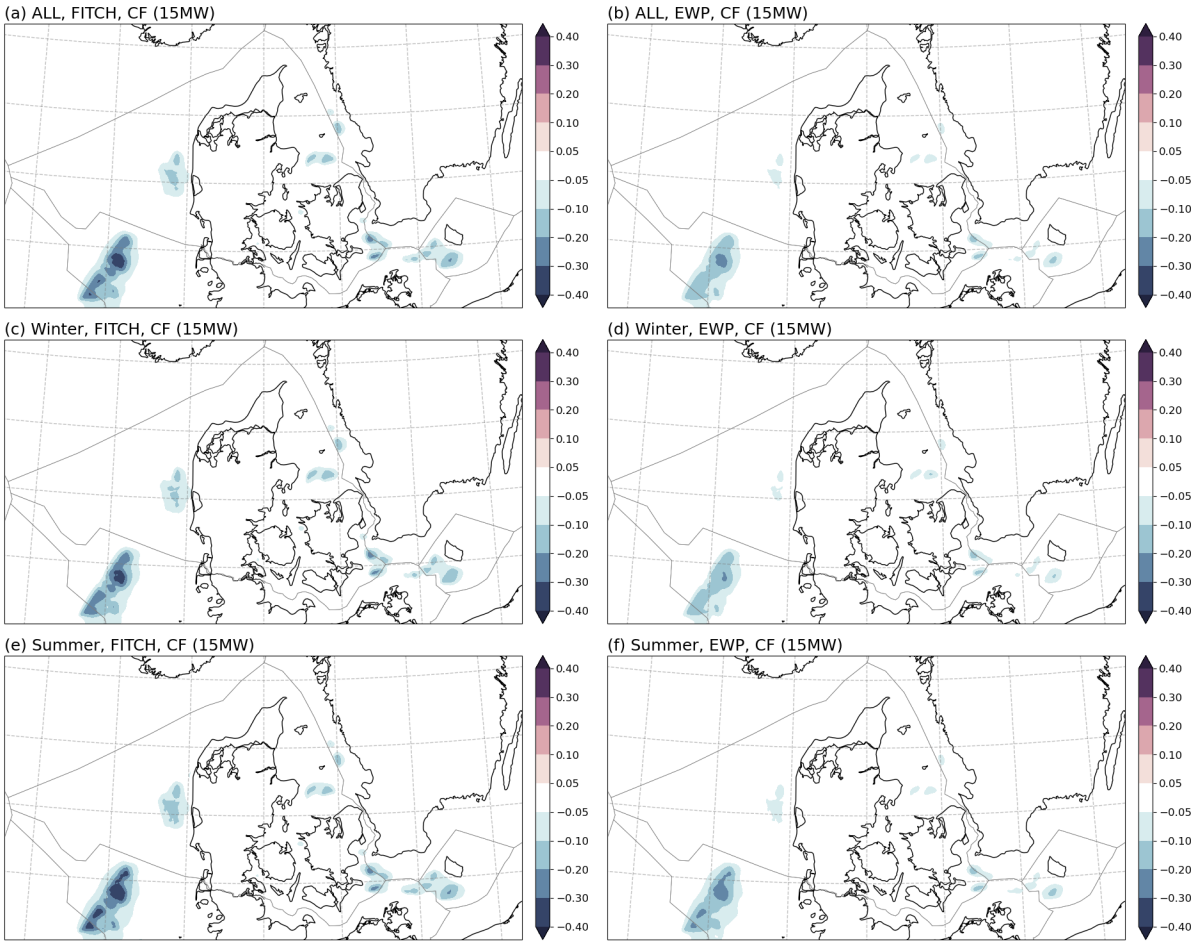

Figure 15: Difference in capacity factor [-] for the IEA 15 MW wind turbine between the Y2030 and CURRENT wind farm scenario for 2019 for the Fitch (a, c, and e) and EWP (b, d, and f) WFPs for the full year (a and b), winter (c and d) and summer (e and f).

The differences in the 15 MW capacity factors (Fig. 15) follow those in the 150 m wind speed. Surrounding the wind farm locations west of Jutland's coast, decreases −0.1 to −0.2 are seen in the Fitch-driven simulations (left column of Fig. 15). Changes in the Danish Baltic Sea in the Kriegers Flak go beyond −0.2 during summer in the Fitch-driven simulation and are smaller in the EWP-driven ones.

Maps for the full domain

The differences in mean wind speed at 150 m and 10 m for the entire domain are presented in Fig. 16 and 17, respectively. At 150 m, differences are most prominent for the Fitch WFP in winter, with values going below −4.0 m s^{-1} at the proposed cluster of wind farms in Scotland.

Figure 17 shows that the decreases in wind speed at 10 m occur at nearly the exact locations as at 150 m but with about half the magnitude. The most significant decreases are seen within the wind farm locations with a range of −1 m s^{-1} to −2 m s^{-1}. However, some areas outside the wind farms experience slight increases in wind speed due to some compensating mechanism. The positive values of the wind speed change at 10 m in a separate colour label with a smaller contour interval, which is more than one order of magnitude smaller than the negative values, with maximum increases of 0.25 m s^{-1} in an area that extends from southern Norway to the middle of the North Sea, where no wind farms are located in the Y2030 wind farm scenario. However, the values are not significant at the 95 % when a rigorous statistical method (e.g., confidence levels determined by block length bootstrapping) is used. The simulations driven by both WFPs show increases that can affect the results of other coupled models, such as wave and hydrodynamic ocean modelling.

The differences in the 15 MW capacity factors (Fig. 18) follow those in the 150 m wind speed. At the wind farm locations in the southern North Sea, substantial differences (~−0.4) are seen in the Fitch-driven simulations (left column of Fig. 18). It is important to note that decreases are generally slightly larger during summer than in the annual mean and winter. While the CF decreases are deeper at the wind farm locations in the Fitch-driven simulations, the area affected by decreases of at least −0.05 (light blue color) is similar in the simulations with both WFPs.

Figure 19 shows the changes in 2-m surface temperatures. There are slight decreases in temperature (~−0.25 °C) over the southern North Sea in the simulations with both WFPs that roughly correspond to the areas with large wind farms in the 2030 scenario with high capacity densities. The area is more extensive in the EWP-driven simulation in winter (Fig. 19d). The physical interpretation of this wind farm cooling is still under investigation, but has previously been reported for large turbines by [21]. There are also areas of slight warming over the Netherlands and northern Germany during summer, consistent with previous studies [21, 33], potentially under smaller wind turbines than those offshore.

Changes in boundary layer height between the CURRENT and Y2030 scenarios are shown in Fig. 20. The boundary layer is defined as that part of the atmosphere that directly feels the effect of the Earth's surface. Depending on the local meteorology, its depth can range from just a few metres to several kilometres. In our simulations, the height of the boundary layer gives a quantitative measure of the depth of the atmosphere directly affected by wind farms. The figure shows increases in boundary layer height in the regions with large offshore wind farms (~120 m) in the North Sea in the Fitch-driven simulations, especially in the summer. The EWP-driven simulations also show increases, but of a more modest magnitude (<30 m). We suspect this is caused by flow adjustment above and around wind farms [42], which is more pronounced when there is added TKE in the Fitch-driven simulations.

The WRF model also estimates the fraction of clouds covering a model grid box. This value is determined by a random overlap of the cloud fraction at each model layer (variable CLDFRAC2D in the WRF model output). The changes in this quantity are shown in Fig. 21. The simulations show increases in cloud fraction near large wind farms in both the Fitch and EWP-driven simulations, especially in winter. In the EWP-driven simulation, the maximum increases are of the order of 7 %. In the Fitch-driven simulations, we find decreases in cloud fractions offshore between wind farms (Fig. 21e). There is likely a relationship between changes in boundary layer height and cloud fraction, but the exact mechanisms are still under investigation. Differences in precipitation between the CURRENT and Y2030 simulations are small and not significant at the 95 % level. Their spatial locations are not directly located around large wind farms.

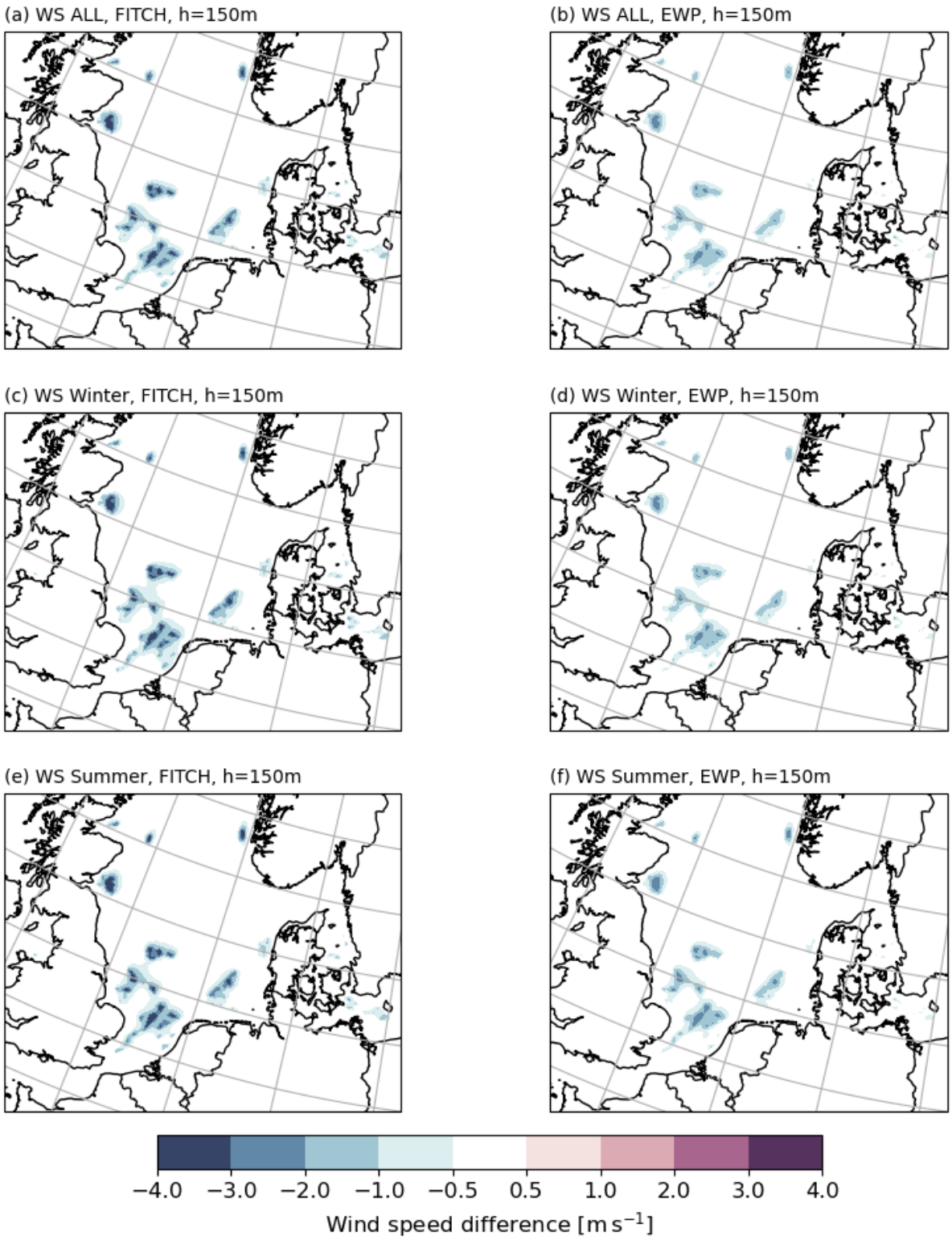

Figure 16: Wind speed difference [m s^{-1}] at 150 m ASL between the Y2030 and CURRENT wind farm scenario for 2019 for the Fitch (a, c, and e) and EWP (b, d, and f) WFPs for the full year (a and b), winter (c and d) and summer (e and f).

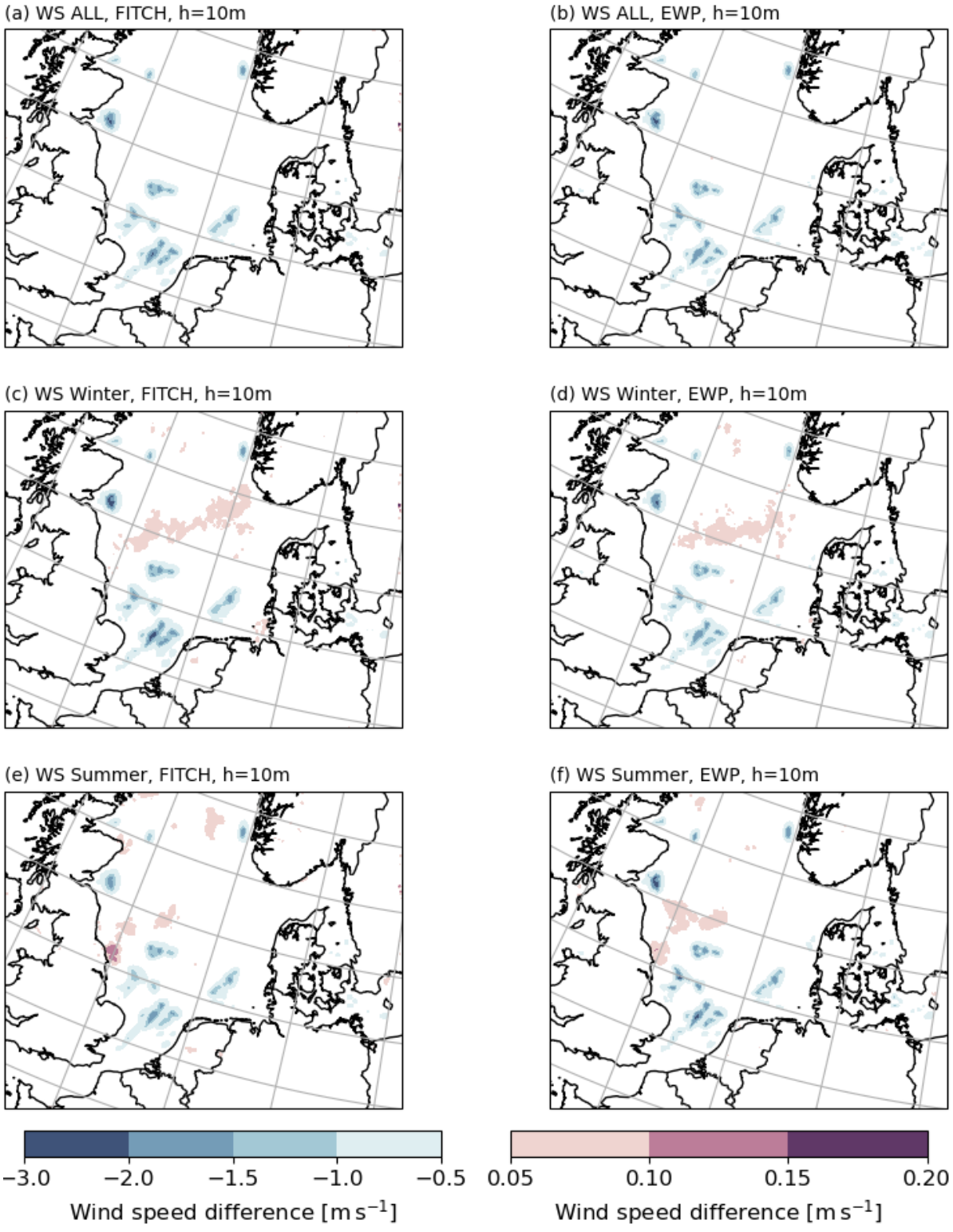

Figure 17: Wind speed difference [m s^{-1}] at 10 m ASL between the Y2030 and CURRENT wind farm scenario for 2019 for the Fitch (a, c, and e) and EWP (b, d, and f) WFPs for the full year (a and b), winter (c and d) and summer (e and f). Note that the positive and negative colour bars have different contour intervals.

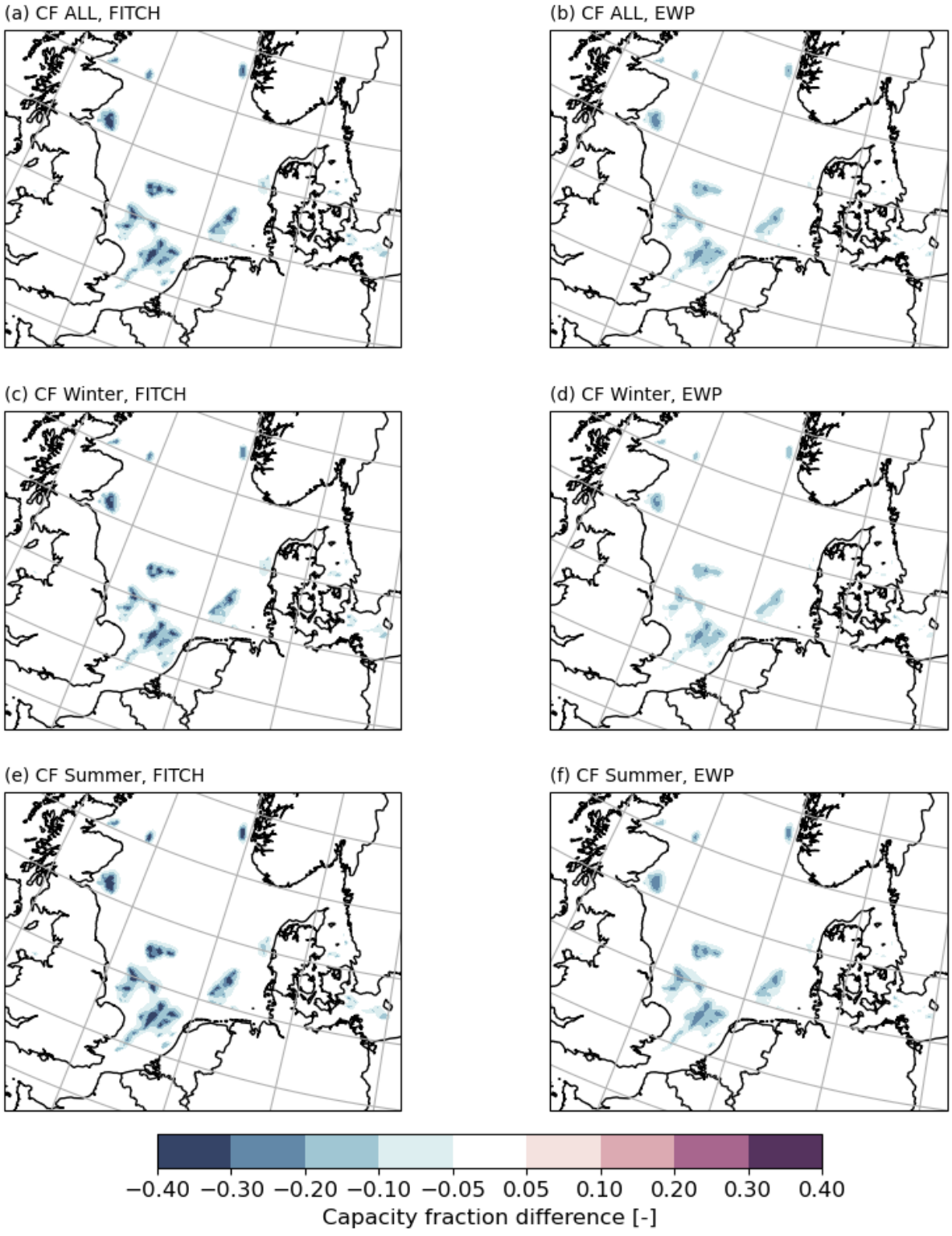

Figure 18: Difference in capacity factor [-] for the IEA 15 MW wind turbine between the Y2030 and CURRENT wind farm scenario for 2019 for the Fitch (a, c, and e) and EWP (b, d, and f) WFPs for the full year (a and b), winter (c and d) and summer (e and f).

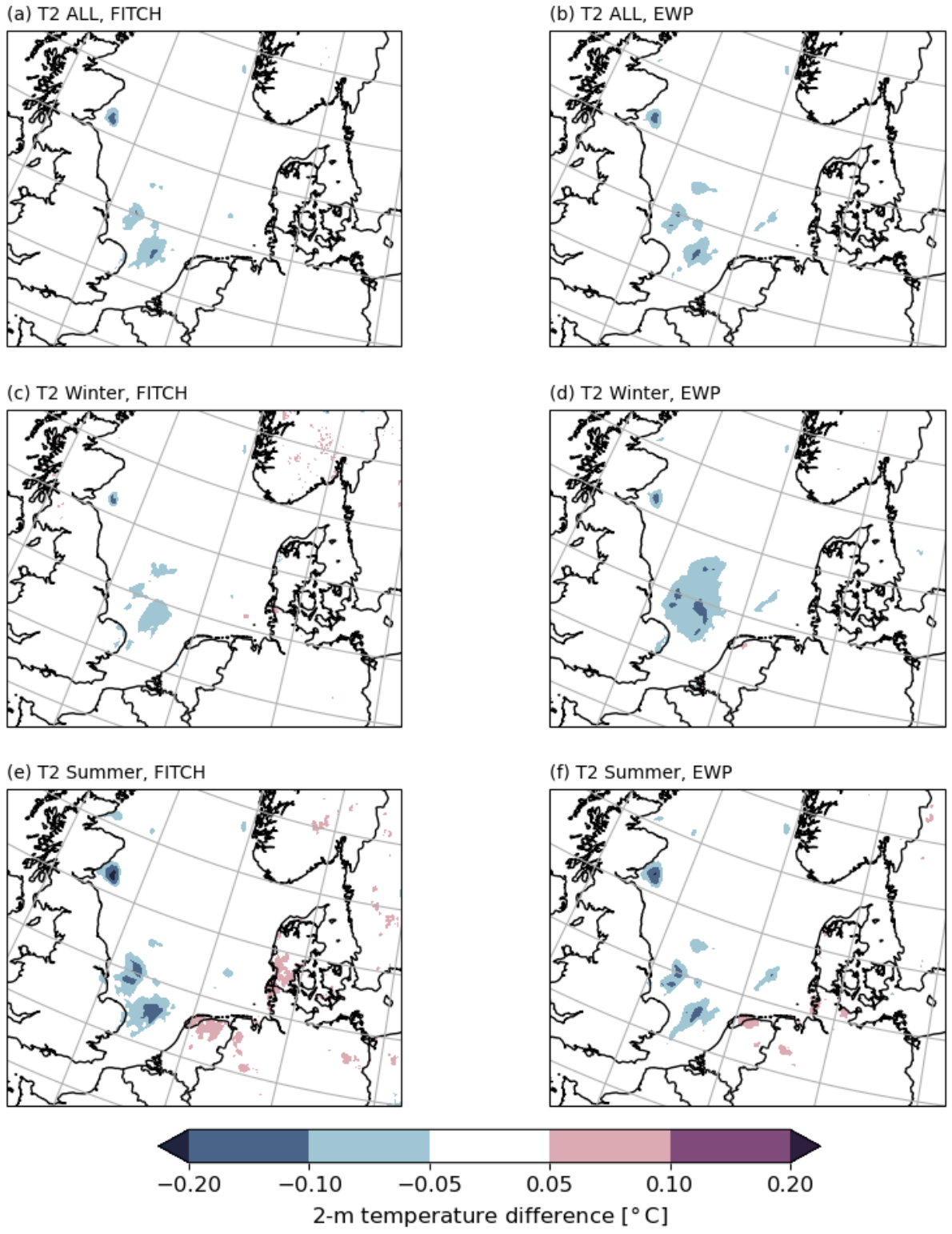

Figure 19: Difference in 2-meter temperature [°C] between the Y2030 and CURRENT wind farm scenario for 2019 for the Fitch (a, c, and e) and EWP (b, d, and f) WFPs for the full year (a and b), winter (c and d) and summer (e and f).

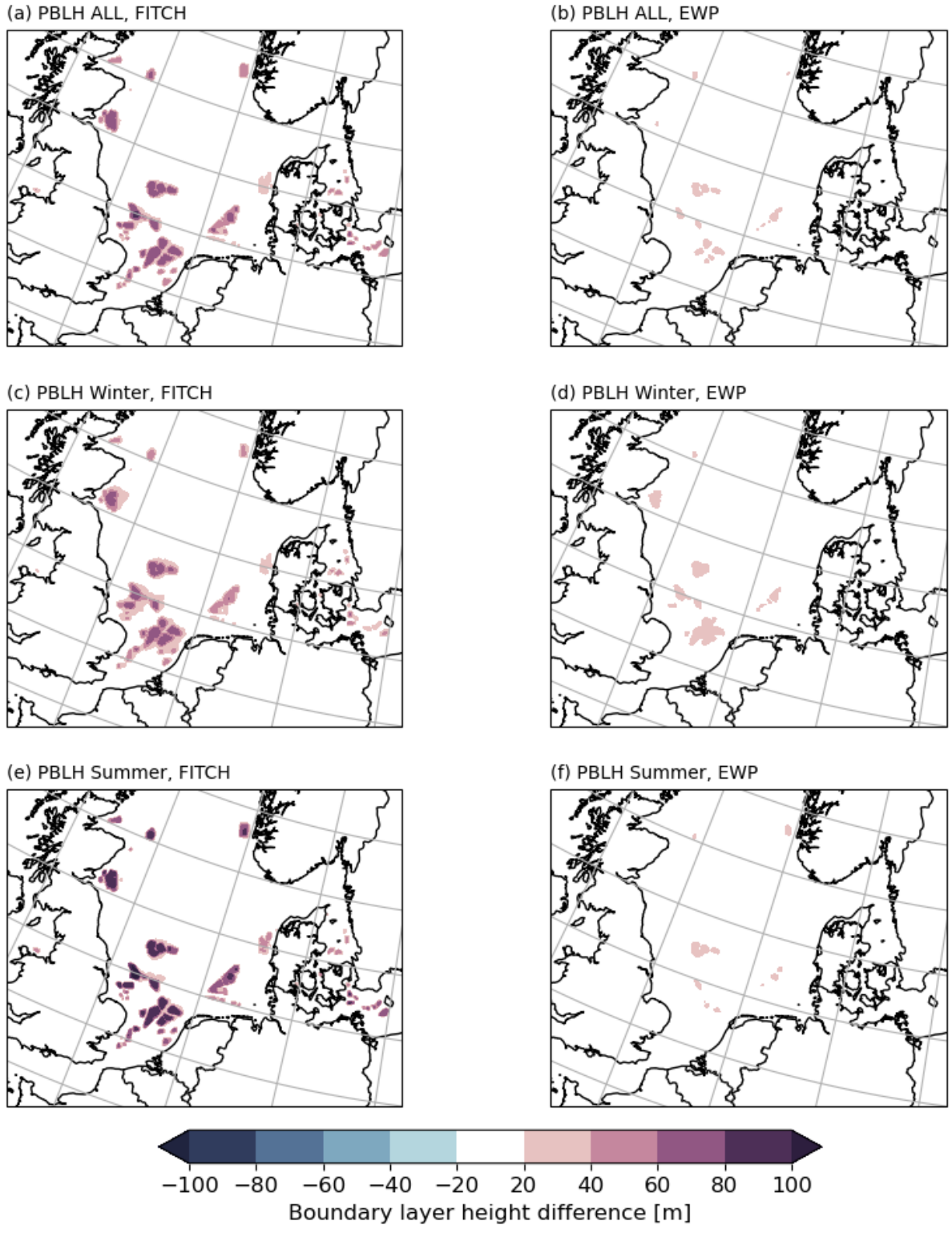

Figure 20: Difference in boundary layer height [m] between the Y2030 and CURRENT wind farm scenario for 2019 for the Fitch (a, c, and e) and EWP (b, d, and f) WFPs for the full year (a and b), winter (c and d) and summer (e and f).

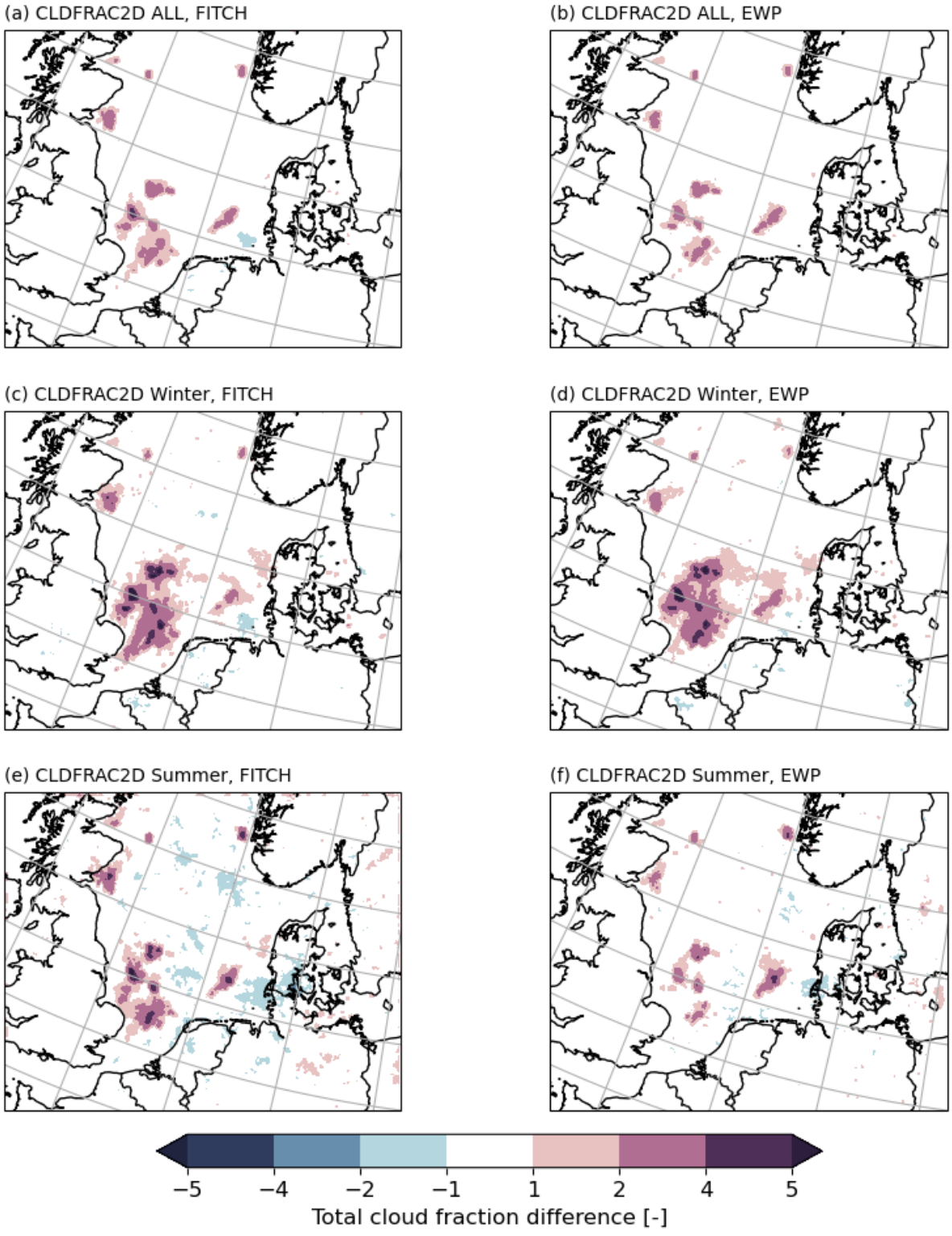

Figure 21: Difference in total cloud fraction [–] between the Y2030 and CURRENT wind farm scenario for 2019 for the Fitch (a, c, and e) and EWP (b, d, and f) WFPs for the full year (a and b), winter (c and d) and summer (e and f).

6.2 Transects through the model domain

To explore the recovery distance downstream of the various wind farms, we construct transects through the WRF modelling domain. The position of the transects is shown in Fig. 22, and the simulation results of five transects in Fig. 23 and Fig. 24.

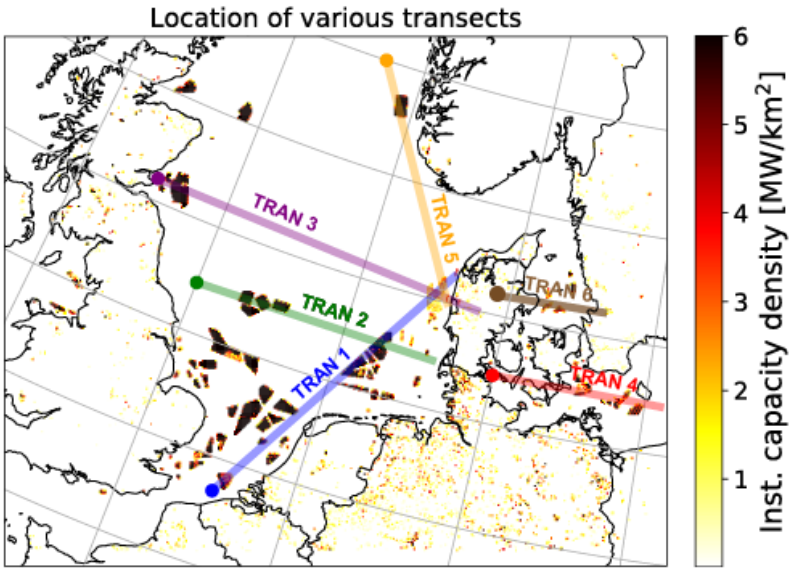

Figure 22: Transect locations in Figs. 23 and 24: Transect 1 (blue), Transect 2 (green), Transect 3 (purple), Transect 4 (red), Transect 5 (orange), and Transect 6 (brown). The dot indicates the origin (i.e., d=0) of the transects.

The transects were drawn by linearly interpolating the annual mean capacity factor in the 2D WRF map to the geographic position of the transect. To facilitate its interpretation, the figures also show the installed capacity density per WRF grid box of the grid box closest to the coordinates of the transect. We take the closest value and not the interpolated one because the effect of the wind farm, which depends on the wind direction of the flow, can be felt beyond the wind farm.

Figure 23 compares the changes in 15 MW capacity factors between the CURRENT and the Y2030 wind farm scenarios. The transects also show the capacity factors (and 0.95 × CF) if no wind farms affected the flow. In Transect 1, which cuts through three current wind farm clusters on the Belgian coast, totalling 706 MW of installed capacity, capacity factors are changed by about −0.15 (i.e., reduced) in the centre of the wind farm. Following the transect northward, the CFs do not return to the No WF values for nearly 250 km because there are wind farms on either side of the transect that are not shown in the figure but influence the wind speed in this region. At about 230 km from the start of the transect, a large cluster of wind farms is encountered in the German Bight in the Y2030 scenario. Wind farms here have very high installed capacities reaching nearly 12 MW km^{-2}. Their wakes reduce the CF from ~0.60 to ~0.35 The distance of 10 km to 20 km between the WFs of the cluster is not enough to recover the flow to pre-wind farm conditions. At the exit of this wind farm, wind speeds quickly recover, and CFs come back to the background level of ~0.65 within 50 km to 60 km.

Transect 2 cuts the central North Sea from west to east. At 100 km, the transect cuts through a large WF cluster with four high installed capacity wind farms (Dogger Bank, Creyke Beck B, Creyke Beck A, Teesside A and B, with 7 GW of combined installed capacity). CFs fall dramatically to about 0.3 at the centre of each WF. The flow returns to a background CF of ~0.6 after about 50 km to 60 km from the eastern edge of the last wind farm. A new wind farm cluster is encountered at about 380 km, which once again reduces CFs to below 0.4 The recovery distance here is longer at this transect with about 60 km to 70 km, likely because there are other smaller wind farms north of the transect.

The third transect is also oriented from west to east, from the Scottish to the Danish coast. CFs fall dramatically after a huge wind farm cluster to nearly the lowest in the North Sea (0.25). The recovery

distance is again about 50 km to 60 km with strong winds and no other wind farms in the vicinity. The transect finally encounters the planned wind farms off the Danish coast with relatively low installed capacity densities (Nordsøen I A1–A3 with a capacity of 6 GW covering a large geographic area). Here, the installed capacity density is about 2 MW km^{-2} to 4 MW km^{-2}, and the CF recovers rather quickly within 20 km to 30 km the expected value of 0.58 at the coast.

Transect 4 goes through the southern Danish islands in the Baltic Sea and towards Bornholm from west to east. The complex of wind farms at Kriegers Flak already reduces CFs from 0.6 to 0.4 in the Y2030 scenario. Further east, the flow does not recover to the undisturbed conditions when it encounters the wind farms of the planned energy island near Bornholm. Here, the CF is reduced to about 0.5 The flow does recover to undisturbed conditions by the end of the modeling domain, nearly 80 km east of the Bornholm energy island.

Transect 5 cuts through the Norwegian coast in a northwest-to-southeast direction. This is the only wind farm in Norway for the Y2030 scenario; it has a planned installed capacity of 10 GW. CFs are reduced to 0.38 at the centre of this wind farm but recover to the background values within 70 km to 80 km. This WF is not expected to influence the CFs along the Danish northwest coast.

Finally, Transect 6 cuts through the Kattegat region with two wind farms in the Y2030 scenario: Kattegat II and Hesselø. The current Anholt wind farm lies north of this transect. The two new wind farms reduce the capacity density from 0.6 to about 0.48. The distance between the two wind farms is too small (about 20 km) for the flow to recover to pre-disturbed conditions.

Figure 24 compares the changes in 15 MW capacity factors between the two Y2030 simulations for the two WFPs. The Fitch WFP simulations generally have much deeper CF reductions than the EWP ones. However, after exiting the wind farm, the recovery distance of the two parameterisations is similar, and the two simulations return to 95 % of the background CF at comparable distances from the downstream edge of the wind farm. This is an expected compensatory mechanism of two parameterisations: the Fitch WFP produces profound wind speed reductions at the wind farm locations. However, because of the addition of TKE, mixing is very efficient and shortens the length of the wakes. In the EWP WFP, the wind speed reductions are smaller within the wind farm, but the wake recovers more slowly due to a smaller momentum mixing from above.

The validity of recovery distances remains unclear due to unvalidated modelling results in various aspects. Comprehensive data to authenticate the simulations is absent because of a lack of extensive observations, and no large wind farms, like those anticipated by 2030, have been constructed yet. Additionally, we have made certain assumptions, such as relatively high horizontal and vertical spacings in the WRF model simulations, to complete the simulations within the designated project timeline. Previous research indicates that reducing the horizontal grid spacing in WRF model simulations could decrease the spatial extent of the wake. Previous research in [39] has shown that grid spacing can affect the results, but a grid spacing of 1 to 3 kilometers was optimal. Additionally, work by [14] has demonstrated that the parameterizations are still helpful and that the WFPs can successfully simulate the median wind resource reductions due to the presence of an upstream farm.

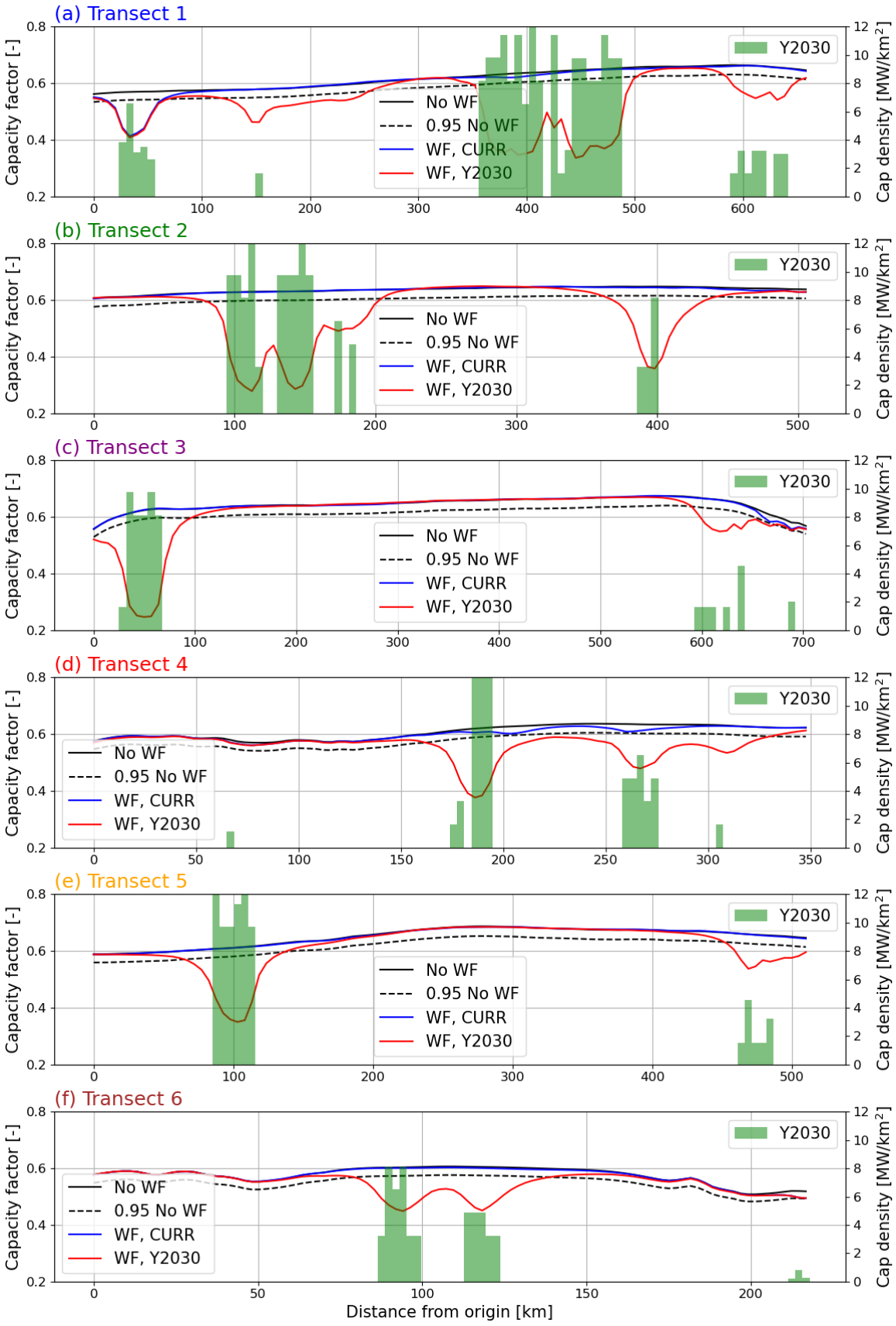

Figure 23: Comparing the 15 MW CF [-] along transects sampling various directions for the CURRENT and Y2030 wind farm scenarios and going through wind farms as shown in Fig. 22 using the Fitch WFP. The green-coloured boxes show the installed capacity density per intersected WRF grid box for the Y2030 scenarios, with the scale on the right. Note that the y-axis starts at a capacity factor of 0.2.

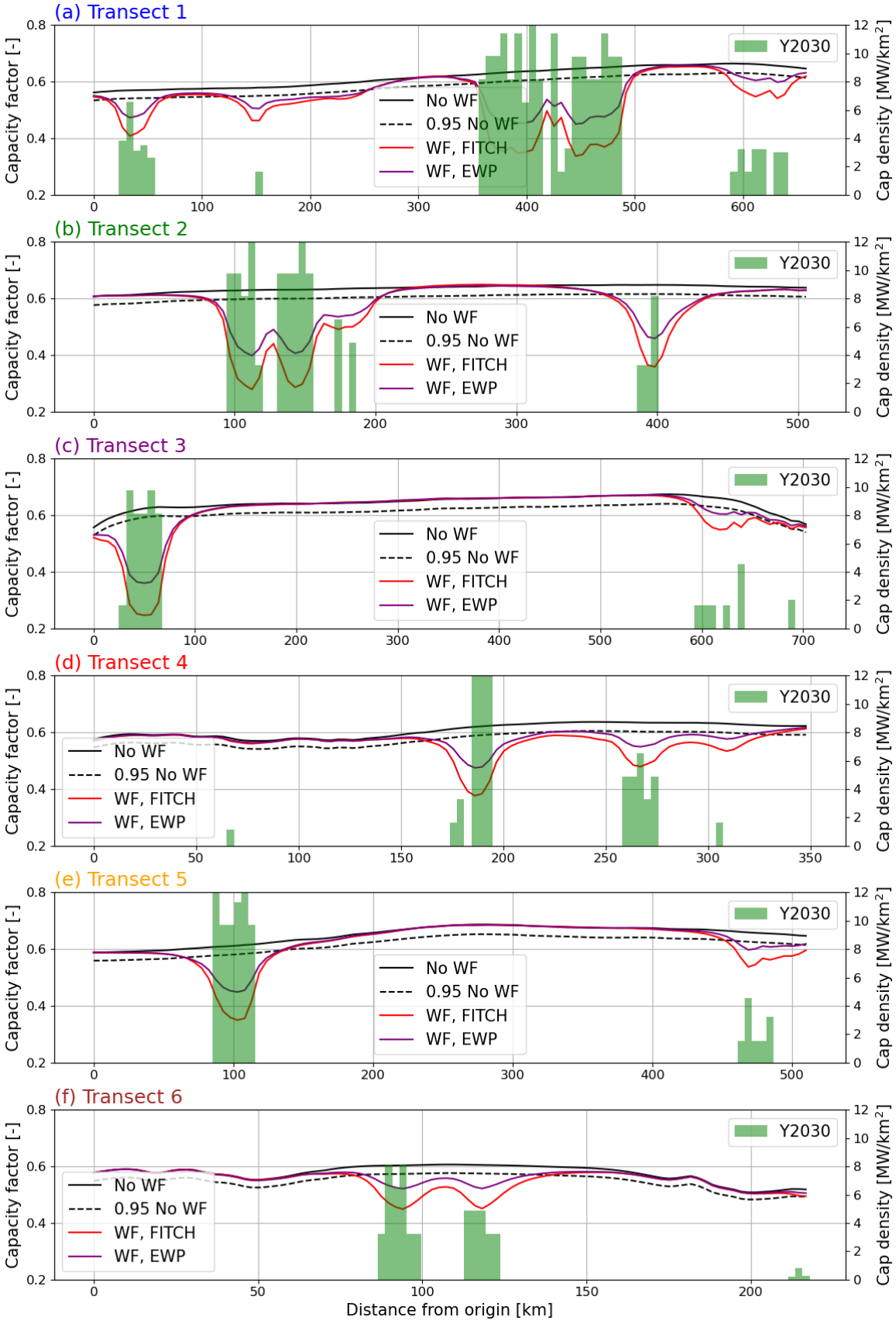

Figure 24: Comparing the 15 MW CF [-] along transects as shown in Fig. 22 for the Fitch (red) and EWP (purple) WFPs and the Y2030 scenario. The green-coloured boxes show the installed capacity density per intersected WRF grid box in the Y2030 scenarios, with the scale on the right. Note that the y-axis starts at a capacity factor of 0.2.

6.3 Wind turbine production

To explore the possible effect of WRF-simulated wakes on power production, we present estimates of the full load hours (FLH) per turbine based on the wind speed simulated in each simulation in Table 2. The load hours are calculated by dividing the (expected) annual energy production calculated from the wind turbine power curve by the nominal power of the wind turbine generator. The theoretical maximum is 8766 FLH, which corresponds to a turbine generating a full nominal power every hour of the year. For reference, a 50 % capacity factor corresponds to 4383 FLH. We also present the wake losses, which are calculated by the relative difference in full load hours between each simulation under a given wind farm scenario and the control (or CURRENT scenario) without wind farms.

The full load hours are calculated by estimating the power a given turbine will generate when subjected to the wind speed simulated at the height of the wind turbine rotor rather than from the power output derived from the WRF model simulations. Regardless of the source, these values include the large-scale wake when the WFP is utilised but exclude other losses such as turbine availability, electrical efficiency, performance, environmental factors, or curtailments. Additionally, some turbine-to-turbine interactions are not simulated by the WFPs if the wind turbines are located within the same WRF model grid cell.

Table 5 summarises the total power production from wind turbines in Denmark, which is approximately 20 TW h (equivalent to 3945 to 4149 annual FLH), produced by an installed capacity of 4751 GW. For reference, the actual annual energy production from wind farms, published by the DEA during the period of 2019–2021, is around 16 TW h [2]. Thus, the simulated production values are reasonable, given that none of the extra losses mentioned above are considered. In 2030, the Y2030 scenario indicates that given an installed capacity of 19.521 GW, Danish wind turbines could produce from 82 TW h to 92 TW h depending on the WFP used in the simulations. Wake losses are estimated as being 12 % to 21 % when using the EWP and Fitch WFPs, respectively.

Table 5: Annual mean full annual load hours and total power production of all Danish turbines in the various simulated scenarios. These values do not include any additional losses due to turbine availability, electrical efficiency, performance, environmental factors, or curtailments.

Wind farm scenario	WFP	Annual mean full load hours	Power production [TWh]
CURRENT	No WF	4404	22.1
CURRENT	Fitch	3945	19.7
CURRENT	EWP	4149	20.8
Y2030	No WF	4867	104.6
Y2030	Fitch	4010	82.0
Y2030	EWP	4370	91.7

As an example of the spatial distribution of the wakes in the various scenarios, we focus on west Jyland, where most offshore wind turbines are located in the Y2030 scenario in Figs 25 to 27.

[2] https://ens.dk/media/6273/download

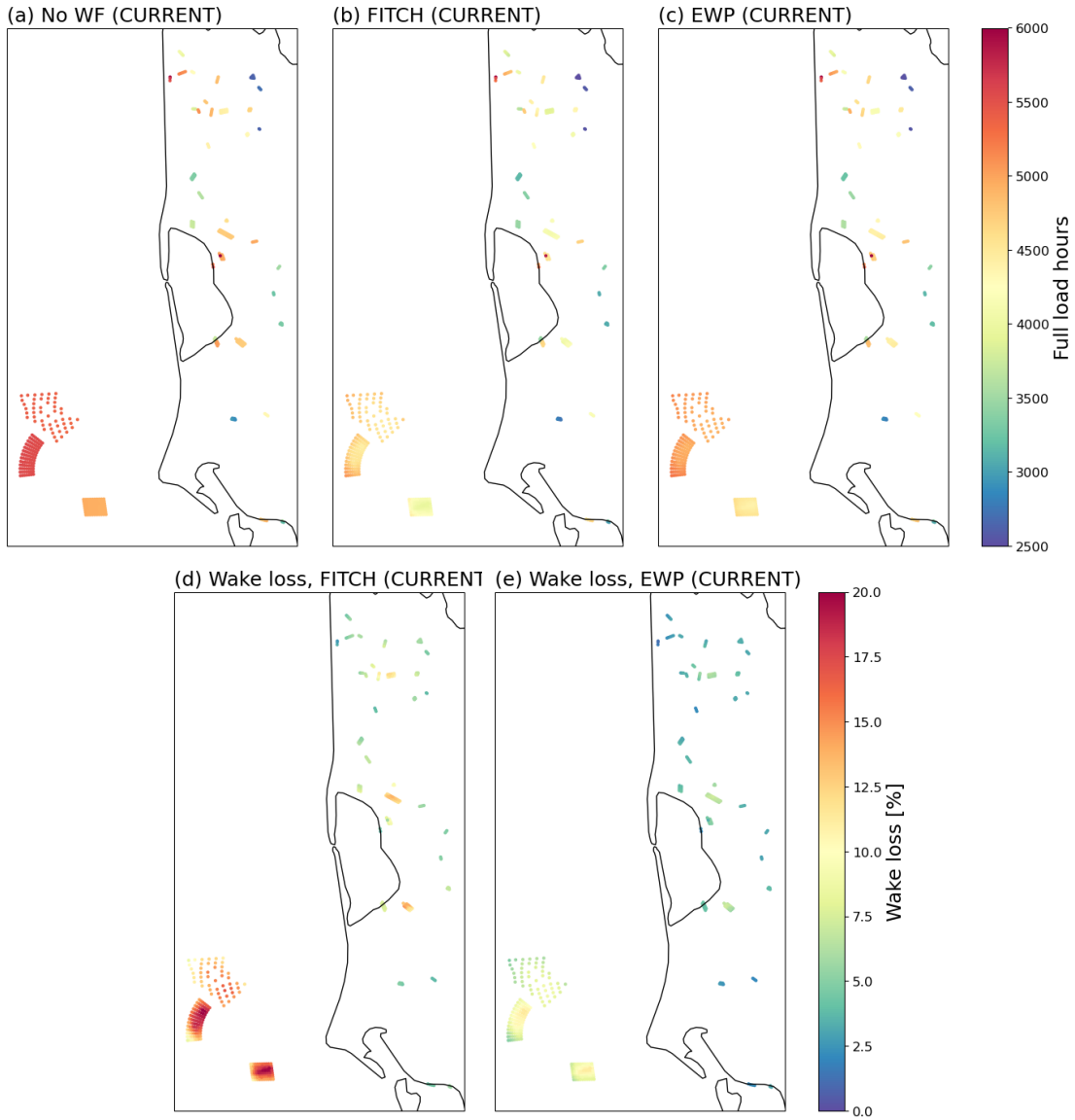

Figure 25: Annual FLHs [h] per wind turbine in the CURRENT wind farm scenario for 2019 for the WRF model simulations using the (a) No wind farm (no WF), (b) Fitch, and (c) EWP WFPs. Wake losses [%] for the CURRENT wind farm scenario for 2019 compared to the no WF simulation for the (d) Fitch and (e) EWP WFPs.

The full load hours estimated from the CURRENT scenario in the No WF, Fitch, and EWP simulations are presented in Fig. 25. Full load hours in the simulations without wake effects vary from 4500 hours at Horns Rev 1 to 5500 hours at Horns Rev 3. Smaller full load values are found onshore where wind speeds are reduced, and the height of the wind turbines is lower. Internal wake losses reduce the full load hours by as much as 20 % at some of the easternmost wind turbines at Horns Rev 1, 2, and 3 in the simulation using the Fitch WFP. In the EWP-driven simulations, the maximum reductions are about ~11 %. The average wake loss for all turbines in the domain shown is 12.0 % and 6.6 % in the WRF simulations driven by the Fitch and EWP WFPs, respectively.

Figure 26 shows the full load hours estimated from the Y2030 scenario using the simulated wind speed from the various WRF model simulations. In the Nordsøen I and Thor wind farms, full load hours vary between 5000 hours to 5700 hours in the Fitch and EWP-driven simulations. The effect of the wake of these wind farms is apparent in the Vesterhavn North and Syd wind farms, with wake losses of nearly 15 % in the Fitch-driven simulation.

Finally, Fig. 27 shows the influence of the Y2030 wind farm scenario on the CURRENT wind farms by subtracting the results of Fig. 26 and Fig. 27. From these simulations, the current wind farms could

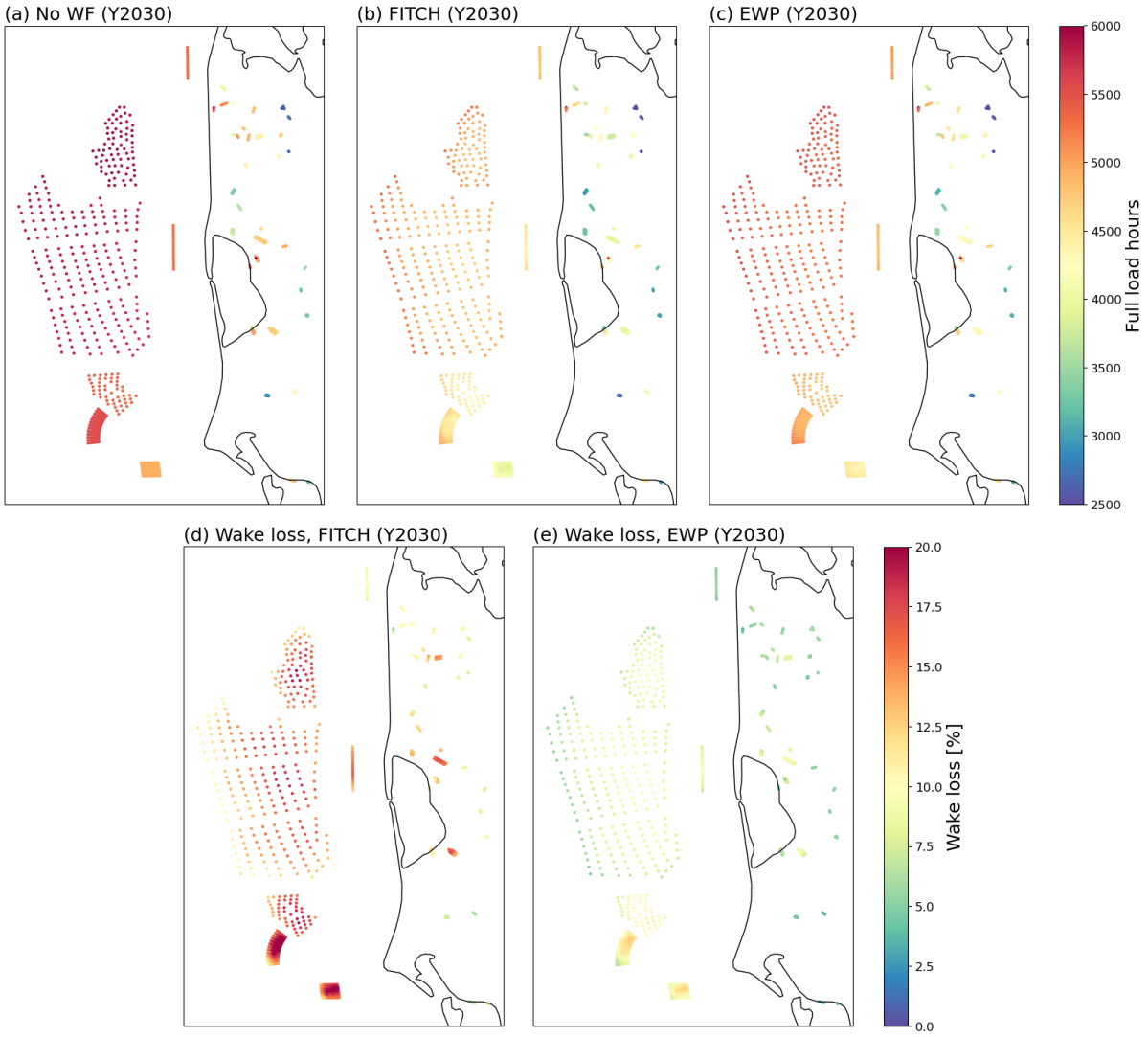

Figure 26: Annual FLH [h] per wind turbine in the Y2030 wind farm scenario for 2019 for the WRF model simulations using (a) No wind farm (no WF), (b) Fitch, and (c) EWP WFPs. Wake losses [%] for the Y2030 wind farm scenario for 2019 compared to the no WF simulation for the (d) Fitch and (e) EWP WFPs.

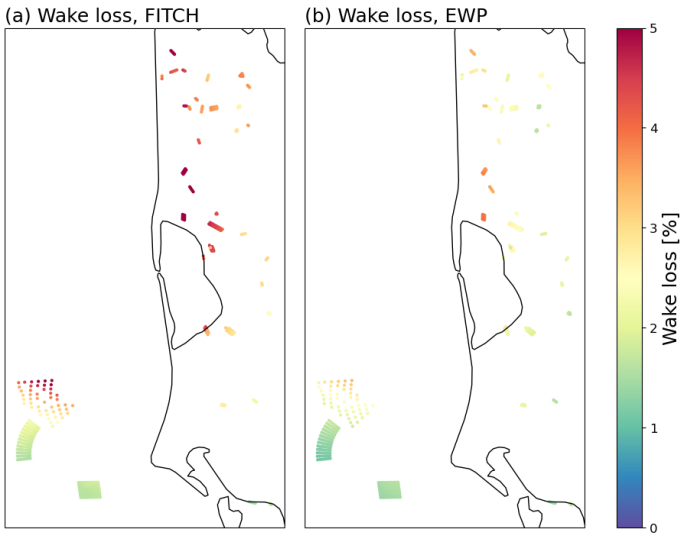

Figure 27: Wake losses [%] for the CURRENT scenario wind farms when the Y2030 wind farms are in operation for the (a) Fitch and (b) EWP WFPs. Note the different color scale range.

be affected on the order of 2 % to 3 % by the Y2030 wind farms, which is well below the losses due to internal wind farm wakes (Fig. 25). On average, wind turbines in this domain have a full load hour of 4192 hours in the CURRENT scenario, which is reduced to 4069 hours in Y2030. The most affected wind turbines are those on land directly west of the large wind offshore wind farms proposed for the North Sea (4–6 %) and the northern edge of Horns Rev 3.

7 Summary and conclusions

The operation of extensive wind farms or clusters of wind farms offshore leads to a marked decrease in wind speed, potentially reaching levels between 1 m s^{-1} to 2 m s^{-1} outside the wind farm area, and this effect can extend from 20 km to 80 km downstream, based on simulations from this study. This phenomenon is known as the large-scale wind farm wake. Internal wakes (i.e., the shadowing effect of one turbine upon other turbines downstream) can reduce wind speeds within large wind farms by up to 4 m s^{-1}, as seen in the complex of wind farms off the Scottish coast. Previous research has suggested that such reductions can considerably impact annual energy production, particularly in regions with high installed capacity density, like the German Bight. To assess wind farm wake losses in the Danish waters, we utilise mesoscale modelling that captures atmospheric conditions and dynamics, accounting for the influence of wind farms and clusters on atmospheric flow.

We simulate the atmospheric flow during 2019 to estimate the wind resources for the North Sea, the South Baltic Sea and the Kattegat using three scenarios: no wind farms, wind farms as installed in November 2021, and future wind farm deployment in 2030. The results of the simulations are compared to one another to understand the impact of wind farms on wind resources. Maps and transects are created to estimate the potential reductions in wind speed, capacity factors, load hours, and the distances needed for the wind to recover to its background values. We also highlight other potential impacts of wind farms on environmental conditions, such as surface temperature, boundary layer height, and cloud fractions.

The main conclusions of this report can be summarised as follows:

- Simulations indicate that in large wind farms planned for a 2030 scenario, wind speeds can be reduced by 4 m s^{-1} and 15 MW capacity factors from 0.6 to 0.2 in the southern North Sea. This region's high installed capacity density drives the large decrease in wind speed (Section 6.1.3; Figs. 7 and 16).
- When focusing on the Danish EEZ, current wind farms and those in the 2030 scenario produce small reductions in hub-height wind speed and capacity factors compared to other regions in the southern North Sea due to strong winds and relatively low installed capacity densities. (Section 6.1; Fig. 13).
- Simulations show that large wind farms can also affect fields other than wind speed at hub height. Our simulations show decreases in 2-m temperature (with a maximum reduction of 0.2 ˚C), increases in boundary layer height (with a maximum raising of 120 m), increases in cloud fractions (with a maximum increase of 7 %). Although the mean annual changes in these quantities are not statistically significant at the 95 %, they could be in certain seasons or under particular stability conditions (Section 6.1.3; Figs. 19, 20 and 21).
- Simulations show that the recovery distances, i.e., the distance required for the CF to return to their background value, for offshore large wind farms vary between 20 km to 80 km. This distance depends on the installed capacity density, the extent of the wind farm, and the background wind speed. In the Danish EEZ, recovery distances are of the order of 20 km to 30 km (Section 6.2 and Fig. 23).
- While the modelling results show a more pronounced impact on the wind speed of large wind farms in the simulations using the Fitch WFP compared to those using the EWP WFP, the recovery distance to the background CF is estimated similarly in both simulations. This is due to different compensatory mechanisms in each WFP, but it does not confirm their validity.
- All the results presented in this report are uncertain because the modelling outcomes remain unvalidated in many respects. No comprehensive data exists to validate the simulations, as extensive observations are lacking, and no large wind farms comparable to those in the 2030 scenario have been established yet (Section 6.2).
- The total power production from wind turbines in Denmark, derived from the WRF model simulations, is ~20 TW h, which is in reasonable agreement with the actual annual energy production of 16 TW h published by the DEA during the period of 2019–2021. Thus, the simulated production values are acceptable, considering that none of the other losses are considered (Section 6.3; Table 5).

References

[1] Agora Energiewende, Technical University of Denmark and Max-Planck-Institute for Biogeochemistry. Making the most of offshore wind: Re-evaluating the potential of offshore wind in the German North Sea. Technical report, Agora Energiewende, 2020.

[2] Karim Ali, David M. Schultz, Alistair Revell, Timothy Stallard, and Pablo Ouro. Assessment of five wind-farm parameterizations in the Weather Research and Forecasting Model: A case study of wind farms in the North Sea. *Monthly Weather Review*, 151(9):2333–2359, August 2023.

[3] Cristina L. Archer, Sicheng Wu, Yulong Ma, and Pedro A. Jiménez. Two corrections for turbulent kinetic energy generated by wind farms in the WRF model. *Monthly Weather Review*, 148(12):4823–4835, 2020.

[4] Nicola Bodini, Simon Castagneri, and Mike Optis. Long-term uncertainty quantification in WRF-modeled offshore wind resource off the US Atlantic coast. *Wind Energy Science*, 8(4):607–620, April 2023.

[5] Nicola Bodini, Mike Optis, Stephanie Redfern, David Rosencrans, Alex Rybchuk, Julie K. Lundquist, Vincent Pronk, Simon Castagneri, Avi Purkayastha, Caroline Draxl, Raghavendra Krishnamurthy, Ethan Young, Billy Roberts, Evan Rosenlieb, and Walter Musial. The 2023 National Offshore Wind data set (NOW-23). *Earth Syst. Sci. Data*, pages 1–57, 2023.

[6] Bundesnetzagentur. Marktstammdatenregister (MaStR).

[7] Neil N. Davis, Jake Badger, Andrea N. Hahmann, Brian O. Hansen, Niels G. Mortensen, Mark Kelly, Xiaoli G. Larsén, Bjarke T. Olsen, Rogier Floors, Gil Lizcano, Pau Casso, Oriol Lacave, Albert Bosch, Ides Bauwens, Oliver James Knight, Albertine Potter van Loon, Rachel Fox, Tigran Parvanyan, Søren Bo Krohn Hansen, Duncan Heathfield, Marko Onninen, and Ray Drummond. The Global Wind Atlas: A high-resolution dataset of climatologies and associated web-based application. *Bulletin of the American Meteorological Society*, 104(8):E1507–E1525, 2023.

[8] Craig J Donlon, Matthew Martin, John Stark, Jonah Roberts-Jones, Emma Fiedler, and Werenfrid Wimmer. The operational sea surface temperature and sea ice analysis (OSTIA) system. *Remote Sensing of Environment*, 116:140–158, 2012.

[9] Martin Dörenkämper, Bjarke T Olsen, Björn Witha, Andrea N Hahmann, Neil N Davis, Jordi Barcons, Yasemin Ezber, Elena García-Bustamante, J Fidel González-Rouco, Jorge Navarro, et al. The making of the New European Wind Atlas –part 2: Production and evaluation. *Geoscientific Model Development*, 13(10):5079–5102, 2020.

[10] Energimyndigheten. Vindbrukskollen – Energimyndigheten, Sweden.

[11] Energistyrelsen. Stamdataregisteret for vindkraftanlæg.

[12] Energistyrelsen. Denmark's largest procurement procedure for offshore wind power is launched, 2024.

[13] European Marine Observation and Data Network (EMODnet).

[14] Jana Fischereit, Roy Brown, Xiaoli Guo Larsén, Jake Badger, and Graham Hawkes. Review of mesoscale wind-farm parametrizations and their applications. *Boundary-Layer Meteorology*, 182(2):175–224, February 2022.

[15] Jana Fischereit, Marc Imberger, and Xiaoli Guo Larsén. Cost-effective mesoscale modeling methods for offshore wind resource assessment with farm wake effect. In *WindEurope Technology Workshop 2022 : Resource Assessment and Analysis of Operating Wind Farms*, 2022.

[16] Jana Fischereit, Xiaoli Guo Larsén, and Andrea N. Hahmann. Climatic impacts of wind-wave-wake interactions in offshore wind farms. *Frontiers in Energy Research*, 10, 2022.

[17] Anna C Fitch, Joseph B Olson, Julie K Lundquist, Jimy Dudhia, Alok K Gupta, John Michalakes, and Idar Barstad. Local and mesoscale impacts of wind farms as parameterized in a mesoscale NWP model. *Mon. Wea. Rev.*, 140(9):3017–3038, September 2012.

[18] Thomas Foken. 50 years of the Monin-Obukhov similarity theory. *Boundary-Layer Meteorology*, 119(3):431–447, 2006.

[19] Evan Gaertner, Jennifer Rinker, Latha Sethuraman, Frederik Zahle, Benjamin Anderson, Garrett E Barter, Nikhar J Abbas, Fanzhong Meng, Pietro Bortolotti, Witold Skrzypinski, et al. Iea wind tcp task 37: definition of the iea 15-megawatt offshore reference wind turbine. Technical report, National Renewable Energy Lab.(NREL), Golden, CO (United States), 2020.

[20] Oscar García-Santiago, Andrea N. Hahmann, Jake Badger, and Alfredo Peña. Evaluation of wind farm parameterizations in the wrf model under different atmospheric stability conditions with high-resolution wake simulations. *Wind Energy Sci.*, 9:963–979, 2024.

[21] Maryam Golbazi, Cristina L Archer, and Stefano Alessandrini. Surface impacts of large offshore wind farms. *Environmental Research Letters*, 17(6):064021, may 2022.

[22] S. Good, E. Fiedler, C. Mao, M.J. Martin, A. Maycock, R. Reid, J. Roberts-Jones, T. Searle, J. Waters, J. While, and M. Worsfold. The current configuration of the OSTIA system for operational production of foundation sea surface temperature and ice concentration analyses. *Remote Sens.*, 12, 2020.

[23] Sven-Erik Gryning, Ekaterina Batchvarova, Burghard Brümmer, Hans Jørgensen, and Søren Larsen. On the extension of the wind profile over homogeneous terrain beyond the surface boundary layer, 2007.

[24] Andrea N Hahmann, Tija Sīle, Björn Witha, Neil N Davis, Martin Dörenkämper, Yasemin Ezber, Elena García-Bustamante, J Fidel González-Rouco, Jorge Navarro, Bjarke T Olsen, et al. The making of the New European Wind Atlas – Part 1: Model sensitivity. *Geoscientific Model Development*, 13(10):5053–5078, 2020.

[25] Charlotte Bay Hasager, James Imber, Jana Fischereit, Aito Fujita, Krystallia Dimitriadou, and Merete Badger. Wind speed-up in wind farm wakes quantified from satellite SAR and mesoscale modeling. *Wind Energy*, n/a(n/a), 2024.

[26] Hans Hersbach, Bill Bell, Paul Berrisford, Shoji Hirahara, András Horányi, Joaquín Muñoz-Sabater, Julien Nicolas, Carole Peubey, Raluca Radu, Dinand Schepers, et al. The ERA5 global reanalysis. *Quarterly Journal of the Royal Meteorological Society*, 146(730):1999–2049, 2020.

[27] Mikio Nakanishi and Hiroshi Niino. An Improved Mellor-Yamada Level-3 Model: Its Numerical Stability and Application to a Regional Prediction of Advection Fog. *Boundary-Layer Meteorol.*, 119(2):397–407, mar 2006.

[28] Michael Nowotny. Recombinator - statistical resampling in python, 2022.

[29] Bjarke T. Olsen, Andrea N. Hahmann, Nicolas G.Alonso-de-Linaje, Mark Zagar, and Martin Dörenkämper. Low-level jets in the North and Baltic Seas: Mesoscale model sensitivity and climatology. *Geoscientific Model Development*, 2025. Preprint.

[30] Bjarke T. Olsen, Andrea N. Hahmann, Anna Maria Sempreviva, Jake Badger, and Hans E. Jørgensen. An intercomparison of mesoscale models at simple sites for wind energy applications. *Wind Energy Science*, 2(1):211–228, May 2017.

[31] OpenStreetMap contributors. Planet dump retrieved from https://planet.osm.org . `https://www.openstreetmap.org`, 2021.

[32] Andreas Platis, Jens Bange, Konrad Bärfuss, Beatriz Cañadillas, Marie Hundhausen, Bughsin Djath, Astrid Lampert, Johannes Schulz-Stellenfleth, Simon Siedersleben, Thomas Neumann, and Stefan Emeis. Long-range modifications of the wind field by offshore wind parks – results of the project wipaff. *Meteorologische Zeitschrift*, 29:355–376, 11 2020.

[33] S. C. Pryor, R. J. Barthelmie, and T. J. Shepherd. 20% of us electricity from wind will have limited impacts on system efficiency and regional climate. *Scientific Reports*, 10, 2020.

[34] S C Pryor, T J Shepherd, P J H Volker, A N Hahmann, and R J Barthelmie. "Wind Theft" from onshore wind turbine arrays: Sensitivity to wind farm parameterization and resolution. *Journal of Applied Meteorology and Climatology*, 59(1):153–174, 2020.

[35] D. Quint, J. K. Lundquist, N. Bodini, and D. Rosencrans. Meteorological impacts of offshore wind turbines as simulated in the Weather Research and Forecasting Model. *Wind Energ. Sci. Discuss. [preprint]*, 2024.

[36] Tristan J. Shepherd, R. J. Barthelmie, and S. C. Pryor. Sensitivity of wind turbine array downstream effects to the parameterization used in WRF. *Journal of Applied Meteorology and Climatology*, 59(3):333–361, 2020.

[37] C. Skamarock, B. Klemp, Jimy Dudhia, O. Gill, Zhiquan Liu, Judith Berner, Wei Wang, G. Powers, G. Duda, Dale Barker, and Xiang-yu Huang. A Description of the Advanced Research WRF Model Version 4.2. Technical Report NCAR/TN-556+STR), NCAR/UCAR, 2021.

[38] The Wind Power. Europe wind farms database.

[39] J. M. Tomaszewski and J. K. Lundquist. Simulated wind farm wake sensitivity to configuration choices in the weather research and forecasting model version 3.8.1. *Geoscientific Model Development*, 13(6):2645–2662, 2020.

[40] P. J.H. Volker, J. Badger, A. N. Hahmann, and S. Ott. The explicit wake parametrisation V1.0: A wind farm parametrisation in the mesoscale model WRF. *Geoscientific Model Development*, 8(11):3715–3731, 2015.

[41] Patrick J H Volker, Andrea N. Hahmann, Jake Badger, and Hans E Jørgensen. Prospects for generating electricity by large onshore and offshore wind farms. *Environ. Res. Lett.*, 12:034022, 2017.

[42] Ka Ling Wu and Fernando Porté-Agel. Flow adjustment inside and around large finite-size wind farms. *Energies*, 10(12), 2017.

ANNEXES

Annex 1 Representative year analysis

To determine the representativeness of calendar year 2019 over the area of interest, 15 locations were randomly selected within the greater North Sea / Baltic Sea area (Fig. 28a). For each location, the time series of wind speed and wind direction at 100 m as well as a proxy for atmospheric stability (seven stability classes based on Obukhov length, reconstructed following [18] and class definition in [23]) covering 1989 to 2021 are downloaded from ERA5 [26]. Annual histograms for each location and variable are computed and compared to a climatological reference based on the complete time series (Figure 28c1 to c3). How close the annual distribution and the reference are is determined using the Earth mover's distance (EMD), which is a commonly used metric for comparing the similarity of two distributions (e.g. [24]). Averaged over all locations, the individual years can be ranked for each variable as shown in Figure 28b.

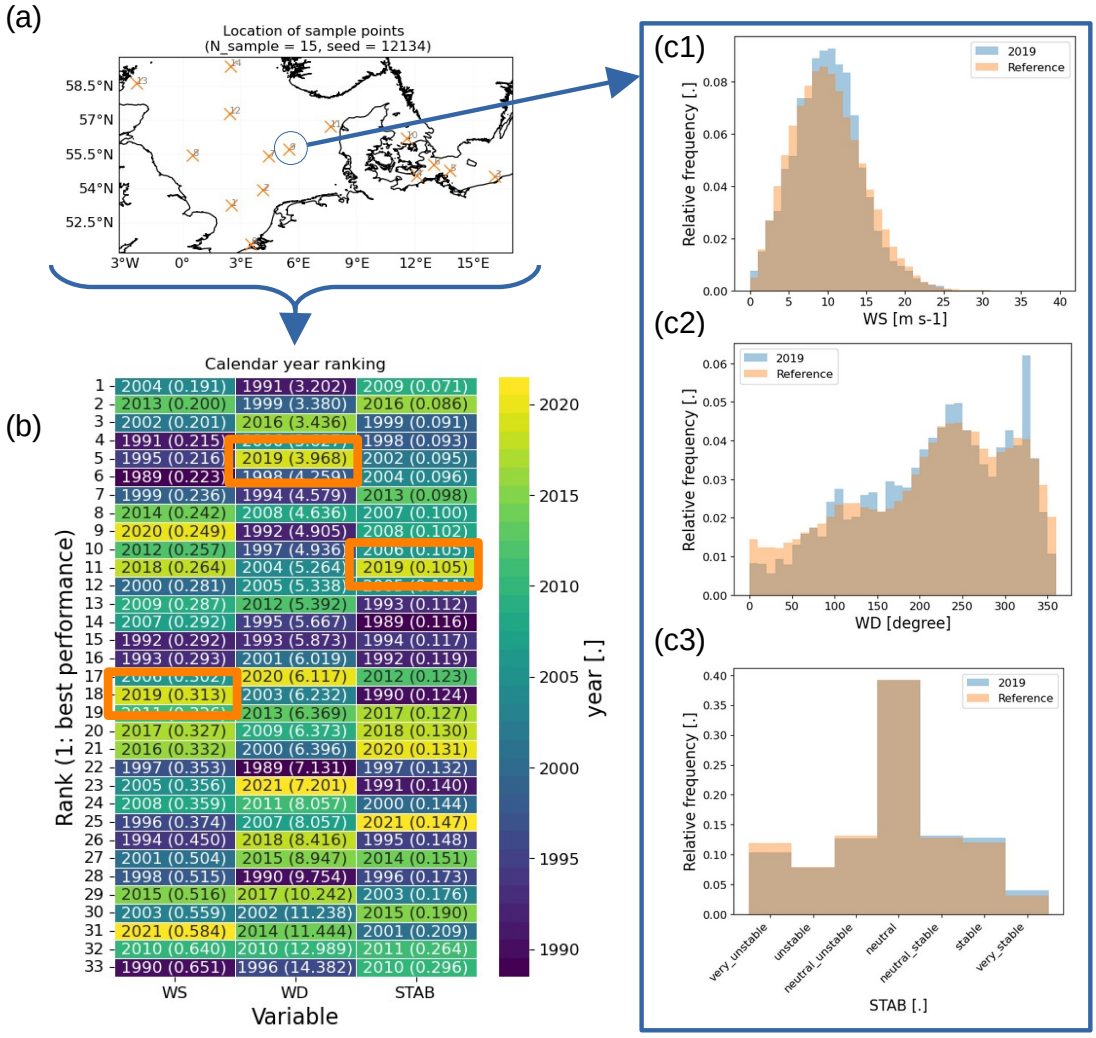

Figure 28: (a) Depiction of the 15 random locations in the focus region of Denmark and the North Sea, (b) Ranking of individual calendar years of wind speed (WS), wind direction (WD) and stability class (STAB) distributions based on their similarity to the long-term average (1989– 2021). 2019 is highlighted in orange. The lower the rank, the higher the similarities. The number in the bracket states the average Earth mover's distance. The histograms of wind speed (c1), wind direction (c2), and stability (c3) compare the calendar year 2019 and the long-term reference year, for example, location #9.